Received: 28 May 2021 | Revised: 23 January 2022 | Accepted: 28 January 2022

DOI: 10.1002/hyp.14508

PROCESSES AND PATTERNS IN TROPICAL HYDROLOGY

WILEY

Tracer-aided modelling reveals quick runoff generation and young streamflow ages in a tropical rainforest catchment

Leia Mayer-Anhalt[1] | Christian Birkel[2,3] | Ricardo Sánchez-Murillo[4,5] | Stephan Schulz[1]

[1]Institute of Applied Geosciences, Technical University Darmstadt, Darmstadt, Germany

[2]Water and Global Change Observatory, Department of Geography, University of Costa Rica, San Jose, Costa Rica

[3]Northern Rivers Institute, University of Aberdeen, Aberdeen, Scotland, UK

[4]University of Texas at Arlington, Department of Earth and Environmental Sciences, Arlington, Texas, USA

[5]Stable Isotopes Research Group and Water Resources Management Laboratory, School of Chemistry, Universidad Nacional, Heredia, Costa Rica

Correspondence
Leia Mayer-Anhalt, Institute of Applied Geosciences, Technical University Darmstadt, Schnittspahnstr. 9, 64287 Darmstadt, Germany.
Email: mayeranhalt@yahoo.de

Funding information
Empresa de Servicios Públicos de Heredia (ESPH); International Atomic Energy Agency, Grant/Award Numbers: COS/7/005, CRP-F31004, CRP-F31005, RC-19747; Research Office of Universidad Nacional (Heredia, Costa Rica); Leverhulme Trust, Grant/Award Number: RPG-2018-375

Abstract

There is still limited understanding of where stream water originates, their flow paths, how water sources mix, and for how long water transits montane tropical catchments. Here, we used a simple gamma convolution integral model (GM), ensemble hydrograph separation (EHS) and a tracer-aided model (TAM) to assess runoff generation, mixing processes and water ages in the pristine tropical rainforest Quebrada Grande catchment in Costa Rica. Model simulations are based on a four-year record (2016–2019) of continuous hydrometric and stable isotope observations. Comparative model tests included multi-objective calibration (2017–2019) and validation (2016) using stream discharge and isotope data as well as an independent model evaluation using groundwater and soil water isotope data. GM and TAM agreed on the dominance of young water in streamflow that was less than 95 days old for 75% of the study period. The EHS suggested a young water fraction threshold of 12 ± 2 days with a transit time distribution that approximates the best-fit GM. These short water ages are the result of high annual rainfall even during drier years such as 2019 with 4300 mm/a and consistent quick near-surface runoff generation with limited mixing. A supra-regional loss (∼55%) of likely older groundwater was detected. The TAM-based hydrograph separation (streamflow KGE > 0.78, δ^2H KGE > 0.90) suggested an average near-surface water contribution of more than 60% to streamflow emphasizing the dominance of quick flow paths. This tropical rainforest represents one of the quickest streamflow responses of mostly young water of pristine catchments globally.

KEYWORDS
Costa Rica, gamma convolution integral model, non-stationary water age, runoff generation, stable isotopes, tracer-aided modelling, tropical rainforest

1 | INTRODUCTION

Central America has been identified as a tropical climate change hot spot (Giorgi, 2006; Gonzalez et al., 2017). For Costa Rica, the IPCC (2021) expects increasing temperatures and decreasing annual precipitation until the end of this century. The Radiative forcing Concentration Pathway (RCP) 8.5 scenario projects an increase in minimum temperatures of about 4°C and an average precipitation

decrease of 31% by the end of the century in Costa Rica (Quesada-Chacón et al., 2021). The already observed temperature and precipitation regime changes in Central America (Aguilar et al., 2005; Knutson et al., 2006) can cause prolonged droughts (Sheffield & Wood, 2008), which result in water scarcity (Bouroncle et al., 2017) and thus endanger ecosystem functioning (Bonal et al., 2016). In Costa Rica, increased precipitation (*P*) variability led to more frequent dry conditions (Hannah et al., 2017) with negative impacts for the agricultural sector and increased water resources conflicts (Esquivel-Hernández et al., 2018; Kuzdas et al., 2014; Kuzdas et al., 2016). Additionally, more frequent heavy rainfall events in the wet season caused flooding in the Greater Metropolitan Area of Costa Rica (Quesada-Román et al., 2021).

The increased risk of hydrometeorological extremes, causing socio-economic losses (Prager et al., 2020), can only be mitigated through measures, whose development requires robust knowledge of hydrological processes, such as runoff generation and groundwater recharge (Bierkens & van den Hurk, 2007). Recent efforts aiming for a better understanding of these processes in Costa Rica (Birkel et al., 2021; Correa et al., 2020; Sánchez-Murillo & Birkel, 2016) are fundamental to allow stakeholders and governments to prioritize efforts, manage resources and establish regulations for watersheds in affected regions (Sánchez-Murillo, Esquivel-Hernández, Corrales-Salazar, et al., 2020). However, in Costa Rica and other tropical countries, hydrological understanding is severely constrained by limited monitoring efforts (Wohl et al., 2012) of the hydrological cycle, particularly in protected and pristine rainforest catchments that provide crucial resources to downstream headwater-dependent systems (Brujinzeel, 2001; Lawrence, 1992; Zadroga, 1981). Quantitative knowledge of the hydrological services provided by rainforests is important to guide conservation efforts such as the operating Payment for Ecosystem Services (PES) scheme (Tognetti et al., 2011) but is currently lacking in Costa Rica. The Quebrada Grande study catchment forms part of such a PES scheme (Wallbott et al., 2019), but has a high mean annual carbon flux (6.7 ± 0.1 g m^{-2} year^{-1}) with high DOC concentrations in streamflow (Figure S1B; Sánchez-Murillo, Romero-Esquivel, et al., 2019).

Assessments of the flow pathways, transit times, and water sources that could be related to DOC transport are crucially missing in this catchment and in most parts of the Latin American tropics (Muñoz-Villers & McDonnell, 2012; Sánchez-Murillo, Romero-Esquivel, et al., 2019). In particular, there are significant knowledge gaps concerning the:

1. timing and magnitude of water storage, exchange between water sources, and the role of deeper hydrogeological systems in volcanic tropical landscapes (Genereux et al., 2013; Osburn et al., 2018; Wiegand & Schwendenmann, 2013);
2. effects of extreme events on discharge-concentration relationships and how solute transport processes, such as mobilization and sorption, are related to discharge rates (Knapp et al., 2020); and.
3. water partitioning under a changing climate (Correa et al., 2020; Iraheta et al., 2021; Sohel et al., 2021).

In this regard, naturally-occurring water tracers (e.g., δ^2H) provide additional information to traditional hydro-meteorological data about the hydrological cycle (Berman et al., 2013; Bony et al., 2008; Bowen, 2008), rainfall-runoff relationship (Uhlenbrook et al., 2002) and hydrogeological connectivity in complex landscapes (Sánchez-Murillo & Durán-Quesada, 2019; Sánchez-Murillo, Esquivel-Hernández, Corrales-Salazar, et al., 2020). If further implemented in TAMs, tracers can – despite inherent model uncertainty (Birkel & Soulsby, 2015) – be a useful tool to assess catchment dynamics of mixing, transport and storage mechanisms, and ecohydrological water partitioning (Hrachowitz et al., 2013; Hrachowitz, Soulsby, Tetzlaff, Dawson, & Malcolm, 2009; Knighton et al., 2017). However, the information gain of the tracer needs to be carefully evaluated against uncertainties arising from calibrated model parameters to incorporate tracer mixing and transport (Uhlenbrook & Hoeg, 2003). Moreover, this information gain often represents a trade-off at the expense of slightly decreased streamflow simulation performance (Delavau et al., 2017; Seibert et al., 2003). TAMs can also be used to track non-stationary water flux ages but do not depend on an a priori defined transit time distribution, which is the case for simpler convolution integral models (Remondi et al., 2018). TAMs as wells as GMs can provide useful information about the catchment's response to environmental changes. Additionally, flux ages are linked to water quality (Sprenger et al., 2019) especially with regard to solutes such as DOC. They thus support an integrated view on catchment functioning and vulnerability (Birkel et al., 2021).

Recently, Kirchner (2016b, 2016a) introduced the "young water" concept since mean transit time (MTT) estimates can suffer from large spatial aggregation errors in heterogeneous catchments. The EHS method allows the determination of water ages and young water fraction thresholds directly from observed input–output tracer series, correlating tracer fluctuations overcoming the need of stationary end-member signatures (Kirchner, 2019; Kirchner & Knapp, 2020).

In order to account for the individual inherent strengths and weaknesses of the previously described methods, we apply all three different model strategies, that is, GM, TAM and EHS, with the comprehensive Quebrada Grande tracer data to compare water age estimates, TTDs and young water fraction thresholds. Upon experience in catchments around the world (Barthold & Woods, 2015), we hypothesized, that this rainforest catchment likely is a well-mixed system with a considerable contribution of older water (Kirchner, 2003; Sidle et al., 2000), resulting in long (>1 year) transit times.

The specific objectives of this study were to:

i. develop, calibrate and independently evaluate a conceptual and relatively simple tracer-aided model capable of simultaneously simulating water and tracer fluxes for a small tropical rainforest catchment;
ii. analyse and compare the estimated TTs from a convolution integral model (GM) in comparison to the TAM-tracked water flux ages and the EHS-derived TTD; and
iii. infer runoff generation and mixing processes from the model tests to obtain an improved understanding of tropical catchment functioning.

2 | STUDY AREA DESCRIPTION

The Wildlife Refuge Cerro Dantas study area is the headwater catchment of the river Quebrada Grande on the Caribbean slope of central Costa Rica and is located within the Braulio Carrillo National Park (Figure 1; Salas-Navarro et al., 2019). The catchment drains towards the Caribbean Sea. Most rocks are of basaltic and andesitic composition due to the location within the Barva volcano complex. This volcanic rock weathers quickly into sandy loam Andosols with relatively high porosity (30%–70%; Macías et al., 2017; Table 1). The groundwater table is on average at 80 cm below the surface (blue triangle, Figure 1; based on field-observations). The saturated hydraulic conductivity of soils sampled across hillslope transects ranges from 50 to 494 mm/day (Sánchez-Murillo, Romero-Esquivel, et al., 2019). A dense bio layer of epiphytes (i.e., mosses, ferns, bromeliads), together with abundant dead plant material, comprises a litter layer of about 20–30 cm on average, resulting in a humic soil cover favouring near surface flow paths.

The vegetation is a mix of primary and secondary forests with minimum anthropogenic activity over the last 100 years (Kappelle, 2016) The mountain stream is characterized by abrupt stream- and riparian slope changes, large cobbles, impacted by debris flows and low electric conductivity (<10 µS/cm; Figure S1A; Sánchez-Murillo, Romero-Esquivel, et al., 2019).

The climate of Costa Rica is mainly influenced by the seasonal movement of the Intertropical Convergence Zone (ITCZ), constant and year-round moisture flow from the north-easterly trade winds, indirect and direct hurricane and tropical storm activities and northern hemisphere cold front outbreaks (Durán-Quesada et al., 2020). Precipitation is also affected by regional oceanic-atmospheric circulations such as the El Niño Southern Oscillation (Table S1; Climate Prediction Center Internet Team, 2020).

The climate in the Quebrada Grande catchment is dominated by the influence of Caribbean trade winds (Table 3; Sánchez-Murillo & Birkel, 2016), causing high humidity close to saturation throughout the year (Figure S2A). There are two precipitation maxima: The first maximum in May/June and the second in August until October. Cold fronts between December and February may also result in large rainfall amounts and cold pulses in air and stream temperature (e.g. Feb 2016, Jan 2018, Figure S2C). The two main maxima are divided by the Mid-Summer Drought in July, so-called "Veranillo" (Magaña et al., 1999; Maldonado et al., 2013), and a slightly drier period from

TABLE 1 Summary statistics of the catchment characteristics, climate, vegetation and soil types in the study area (Murillo et al., 2019; Ortiz-Malavasi, 2014)

Physiographic characteristic (unit)	Mean (range)
Topography	
Area (km^2)	3.9
Stream length (km)	4.0
Catchment length (km)	3.6
Slope (°)	9.59 (1 to 43)
Altitude (m.a.s.l.)	2222 (1765 to 2350)
Climate and vegetation	
Climate zone	Humid tropics (Aw)
Land use	Montane rainforest
Soil type (Table S2)	Andosols (young volcanic soils)

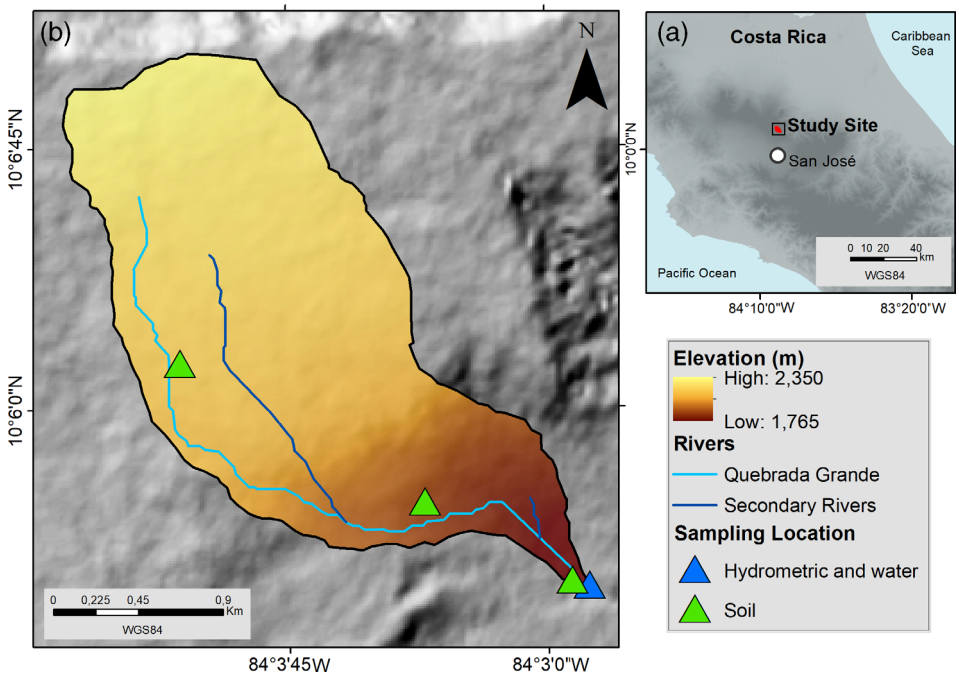

FIGURE 1 Regional overview of the study area with elevation from a national 10 m grid digital elevation model and sampling locations (b) and location within Costa Rica (a)

TABLE 2 The TAM model flux equations with starting parameter values and parameter intervals used for model calibration

Flow direction	Equation	Model parameter	Starting value	Parameter interval
Hillslope → Riparian area	$Q_{up} = a^*S_{up}$	a (d^{-1})	0.21	0.1–0.9
Groundwater → Q_{sim}	$Q_{GW} = b^*S_{GW}$	b (d^{-1})	0.009	0.0001–0.1
Hillslope → Groundwater	$Q_R = R^*S_{up}$	R (d^{-1})	0.5	0.1–0.9
Riparia area → Q_{sim}	$Q_{rip} = c^*S_{rip}^{(1+\alpha)}$	c (d^{-1})	0.019	0.0001–0.5
		α (–)	0.2	0.1–0.9
Isotope mixing volumes				
		MV_{up} (mm)	1000	1–2000
		MV_{rip} (mm)	1	1–500
		MV_{GW} (mm)	1	100–5000

TABLE 3 Summary of measured hydrometric data and isotope ratios in rain-, soil-, stream- and groundwater (GW) with the number of samples (*n*)

Hydrometric data (mm)	Period	Mean	Range	
Annual precipitation	2016–2019	5117	4314–6146	
Annual evapotranspiration	2016–2019	612	555–653	
Annual stream discharge	2016–2019	1596	918–1947	
Isotope ratios (‰)	**Period**	**Mean**	**Range**	***n***
δ^2H in rain	2016–2019	−30.36	−161.0 to +21.3	914
δ^2H in soilwater	2018	−44.51	−112.3 to −27.7	15
δ^2H in GW	2019	−33.67	−37.5 to −28.0	9
δ^2H in stream	2016–2019	−30.34	−79.2 to −1.4	414
$\delta^{18}O$ in rain	2016–2019	−5.42	−21.1 to +0.7	914
$\delta^{18}O$ in soilwater	2018	−6.94	−14.8 to −5.0	15
$\delta^{18}O$ in GW	2019	−5.67	−6.8 to −4.2	9
$\delta^{18}O$ in stream	2016–2019	−5.55	−12.0 to −2.3	414

mid-February to April. The drier months are accompanied by higher irradiation (Figure S2B).

3 | METHODS AND DATA

3.1 | Sampling and data

The catchment has been intensively monitored since October 2015; this includes data on meteorology, streamflow, physical soil properties, and water chemistry and isotopic composition. Meteorological data (precipitation, air temperature, relative humidity, solar radiation and wind speed) is recorded every 30 min at a Vantage Pro2 Plus weather station (Davis Instruments, USA; blue triangle, Figure 1). Actual evapotranspiration (ET) was estimated using a vegetation-adapted version of the Penman-Monteith equation and the assumption that there is unlimited water availability (Allen et al., 1998). Stream stage and temperature are logged every 15 min with a pressure transducer combined with a thermometer (AS950, Hach). Once per week, discharge ($n = 138$) is measured by a tracer test, that is, analysing the breakthrough curve of an instantaneous salt injection (Moore, 2005) since high channel roughness precludes the use of flow meters. This data enabled us to derive a robust stage-discharge relationship (rating curve and resulting hydrograph in Figure S3) for water balance calculations (Sánchez-Murillo, Romero-Esquivel, et al., 2019).

The stable isotopes δ^2H and $\delta^{18}O$ of daily rainfall were sampled using a passive collector (Palmex Ltd, Croatia; Gröning et al., 2012). Stream water was sampled daily in 2016 using a Sigma 900 MAX autosampler (HACH, USA) and weekly (manual sampling) from 2017 to 2019. Groundwater samples were collected by manually purging a 1 m deep dug-well, which was covered with a PVC stopper during rainfall events. The well is located in the riparian zone (Figure 1), which remained saturated year-round, and is considered representative for the lower part of the catchment. All samples were stored until analysis at 5°C in 30 ml bottles with no headspace and hermetically sealed to avoid exchange with atmospheric moisture. Prior to analysis, all samples were filtered with a 0.45 μm syringe polytetrafluorethylene (PTFE) membrane.

Soil samples (500 g) were collected weekly in 2018 at a distance of 25–30 m from the stream channel at 15 cm depth below the humic soil cover (Figure 1) and stored in sealed polyethylene bags at 5°C.

Soil sampling locations were selected randomly based on access to represent the lower, middle, and upper part of the catchment (-Table S2). Sub-samples were transferred to 50 ml tubes (Eppendorf, Germany) and centrifuged at 5°C and 11 000 rpm for 1.5 h using a 5804 R centrifuge (Eppendorf, Germany) to extract the mobile water content. The supernatant water was extracted with a micropipette (Eppendorf, Germany), filtered through a 0.45 µm PTFE filter and transferred into a 2 ml injection vial.

Stable isotope analysis was conducted at the Stable Isotopes Research Group facilities of the Universidad Nacional, Costa Rica using a Cavity Ring-Down Spectroscopy water isotope analyser (L2120-i, Picarro Inc.) and a water isotope analyser (LWIA-45P, Los Gatos Research Inc.). The long-term analytical uncertainty was ±0.5‰ for δ^2H and ±0.1‰ for δ^{18}O (Ramírez-Leiva et al., 2017). Spectral contamination identification was applied to soil samples to avoid organic interference on isotope ratios (Schultz et al., 2011; West et al., 2011). The few data gaps (<5%) were interpolated to provide a continuous daily isotope dataset for the complete period 2016–2019. Stable isotope ratios are presented in delta notation δ^{18}O [‰] and δ^2H [‰] relating the ratios of ^{18}O/^{16}O and ^{2}H/^{1}H to Vienna Standard Mean Ocean Water.

The isotopic composition of rainwater is influenced by the amount and the altitude effect (Sánchez-Murillo, Esquivel-Hernández, Birkel, et al., 2020). Our isotope sampling does not account for the 500 m catchment elevation range that could result in an average depletion of around −1‰ δ^{18}O (Sánchez-Murillo et al., 2013). However, the altitude effect is comparatively low to the observed inter-annual isotopic variation in rainfall of 22‰ δ^{18}O (Table 3). Moreover, the isotopic composition of unsampled throughfall might differ from the isotopic composition of gross precipitation used for model input due to, for example, (i) evaporative fractionation from the canopy, (ii) diffusive exchange with ambient vapour, and (iii) selective transmittance of temporally varying rainfall (Allen et al., 2017). Analysing 21 studies in different environments, Allen et al. (2017) could show that the isotopic signature of throughfall is usually slightly enriched compared to gross precipitation. However, the reported differences are almost always well below 1‰ δ^{18}O and on average only +0.25‰ δ^{18}O. Additionally, Soulsby et al. (2017) indicated that evaporative fractionation of intercepted water is restricted to low rainfall volumes, which are rather untypical in our catchment with 5000 mm annual precipitation. Also, in humid forests with dense vegetation, a constantly high relative humidity and reduced solar radiation due to cloud cover (Dehaspe et al., 2018) maintains a wet canopy for longer time periods limiting evaporative fractionation (Aparecido et al., 2016; Correa et al., 2020). These specific conditions in our rainforest catchment give reason to assume that sampling errors in the input isotope ratio do not exceed analytical measurement errors.

3.2 | Gamma convolution integral transit time model

The simple convolution integral transit time model (Equation 1) estimates stream isotope ratios with corresponding TT:

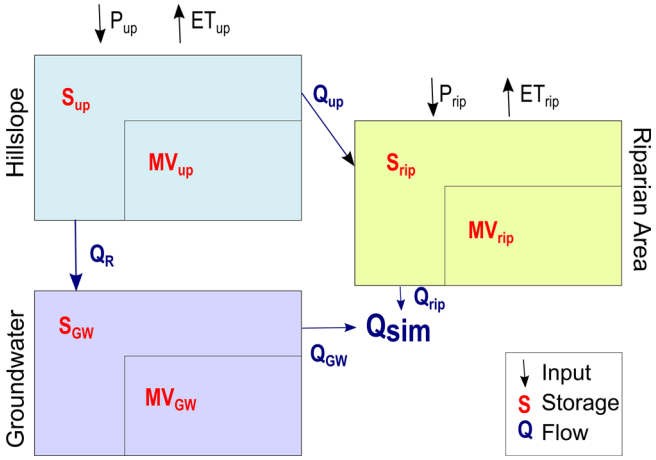

FIGURE 2 The TAM uses precipitation (*P*) and evapotranspiration (ET) data and divides the catchment in a hillslope and riparian wetland storage fraction to simulate streamflow (Q_{sim}) and streamflow deuterium dynamics. The three dynamic storages (S_{up}, S_{rip}, S_{GW}: Upper, lower and groundwater) contribute water (Q_{up}, Q_{GW}, Q_R, and Q_{rip}) to Q_{sim} with additional mixing volumes (MVs) for tracer transport using a mass balance approach

$$\delta_{out}(t) = g(t) * \delta_{in}(t-\tau) = \int_0^{\infty} g(\tau)\delta_{in}(t-\tau)\, d\tau \quad (1)$$

This model converts the input of daily isotopic composition of precipitation into an approximation of the stream isotope ratios $\delta_{out}(t)$ using a transfer function $g(\tau)$. The daily evapotranspiration was subtracted from the daily precipitation amount for the input function δ_{in} $(t-\tau)$ of the convolution integral, assuming that surface water is not affected by fractionation. This assumption is supported by the stream water isotope samples plotting consistently close to the Local Meteoric Water Line (LMWL; Figure 3) with *d*-excess (Mean ± SD) values

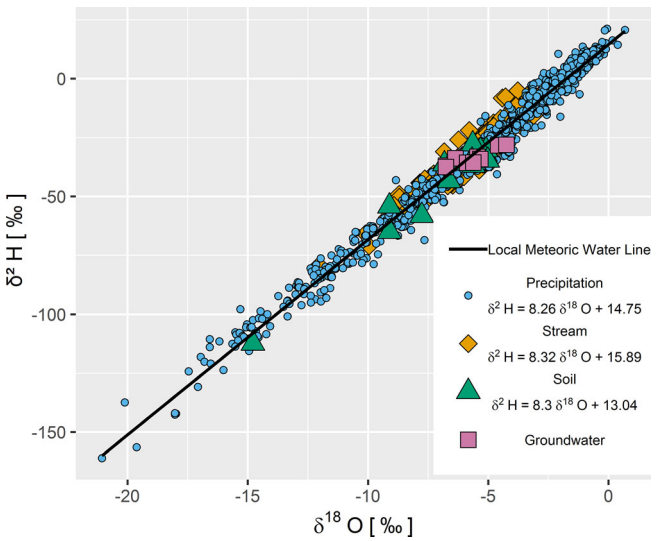

FIGURE 3 Local meteoric water line of the Quebrada Grande study area and stable water isotope signatures of stream-, soil- and groundwater with regression equations

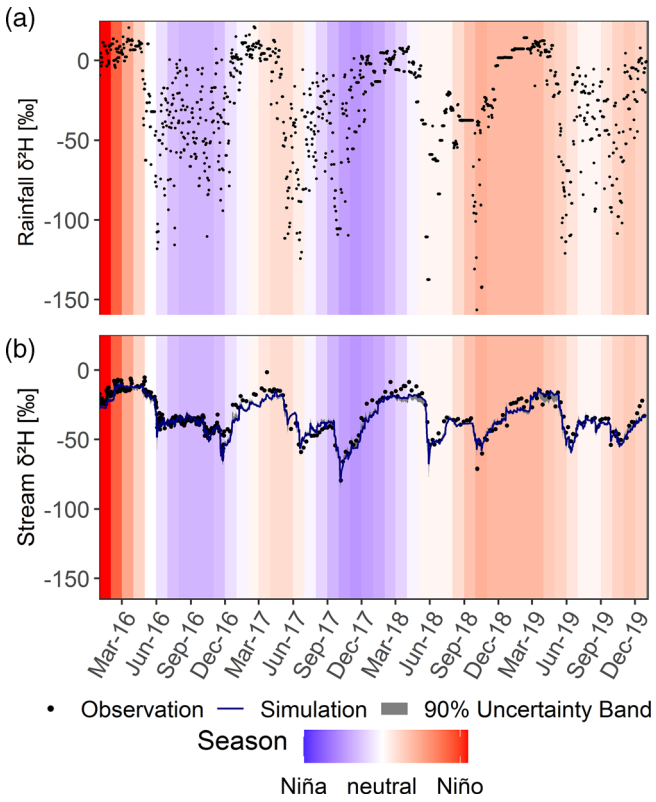

FIGURE 4 Gamma model results: (a) input data of observed deuterium (δ^2H) in rainfall (black dots) and (b) in streamwater δ^2H (black dots), as well as streamwater simulations with 90% uncertainty band (blue line with grey band). The shaded background represents the classified El Niño/La Niña events (Table S1; Climate Prediction Center Internet Team, 2020)

ranging from 3.8‰ to 27.1‰ (14.1 ± 3.5‰) and lc-excess of −9.7‰–13.5‰ (0.8 ± 3.5‰) (Landwehr & Coplen, 2018). Previous work by Sánchez-Murillo, Romero-Esquivel, et al. (2019) tested a simple exponential distribution as transfer function $g(\tau)$ for data from 2017. In this study, we settled on the more versatile two-parameter gamma distribution, following Hrachowitz, Soulsby, Tetzlaff, Dawson, Dunn, and Malcolm (2009):

$$g(t) = \frac{\tau^{\alpha-1}}{\beta^{\alpha}\Gamma(\alpha)} \exp\left(-\frac{\tau}{\beta}\right) \quad (2)$$

where α (−) is the shape parameter and β (days) the scale parameter. The GM assumes steady-state, which is rarely the case for catchment-scale hydrological processes (McGuire & McDonnell, 2006). However, given the fact that it relies on only two calibrated parameters, it allows for a simple model test and traceable uncertainty.

The GM model was calibrated for the entire study period (2016–2019) and for every single year individually with a looped 3-years warm-up period. The Mean Transit Time (MTT) was calculated based on the best-fit α and β parameters for the different periods. Due to the limitations of stable water isotopes to detect transit times exceeding 5 years (Stewart et al., 2010), the scale parameter was limited to 1825 days. We attempted to select the best 100 parameter sets of the simulations based on the Nash-Sutcliffe-Efficiency (NSE; Nash & Sutcliffe, 1970). The Differential Evolution algorithm (DEoptim R package; Ardia et al., 2020) was used for calibration with a maximum of 10 000 iterations, starting values of α and β of 0.5 and 1000 days, respectively, and a stop criterion of a NSE of 0.01. The simulation results were visualized with the mean and 90% percentiles (uncertainty bands) of the best performing parameter sets (Figure 4).

3.3 | Tracer-aided model calibration and evaluation

The conceptual tracer-aided hydrological model (TAM) simultaneously simulates streamflow (Q_{sim}) and the stream isotope ratio (δ^2H). It was set up according to previous empirical knowledge by Sánchez-Murillo, Romero-Esquivel, et al. (2019) using geochemical data. Their conceptual model includes shallow runoff generation via a saturated riparian area and a slightly deeper (<1 m) more constant interflow contribution to streamflow (Figure 2). This translates into a linear upper reservoir (S_{up}) draining into a lower reservoir (S_{GW}) generating groundwater flow (Q_{GW}) to the stream. The S_{up} provides runoff (Q_{up}) to the riparian reservoir (S_{rip}; using the linear parameter a) that generates saturation overland flow (Q_{rip}) contributing to Q_{sim} with the non-linear parameter α.

The isotope mass balance (Figure 2) is coupled with a mixing-cell approach to the dynamic water storage and transport of the rainfall-runoff (Table 2). Three calibrated mixing volumes (MV_{up}, MV_{GW}, and MV_{rip}) for each of the three storage volumes (S_{up}, S_{GW}, and S_{rip}) contain the isotope ratio for complete mixing and transport without affecting the water storage and transport:

$$\frac{d(cS)}{dt} = \sum_j c_{I,j} I_j - \sum_k c_{o,k} O_k \quad (3)$$

where c is the isotope ratio (‰) in j storage inflows I_j components (e.g., P_{up} and P_{rip}, Q_{up}, Recharge Q_R) and k outflow O_k components (e.g. ET_{up} and ET_{rip}, Q_{GW}, and Q_{rip}), which characterize the catchment storage S dynamics (sum of dynamic and additional storage available for mixing) and associated isotope ratios c. The model storage isotope ratios were initiated with the mean of measured (soil, stream, groundwater) isotope values of corresponding storages and storage volumes of 1 mm. The year 2016 warm-up period was sufficient to fill storages and omitted from calibration. The eight parameter intervals used for calibration are based on model tests and previous applications (Table 2).

We used the non-sorting dominated multi-objective genetic algorithm (NSGA2) with 500 parameter populations over 100 generations with a total of 50 000 iterations in each step for reproducibility (Deb et al., 2002). The model performance was evaluated using the Kling-Gupta Efficiency (KGE; Gupta et al., 2009; Kling et al., 2012; Zambrano-Bigiarini, 2020) accounting for the correlation coefficient (r), variability (γ) and bias (β) (Equation (4)):

TABLE 4 The water balance (precipitation *P*, the vegetation adjusted PET and observed streamflow Q_{obs}), the derived water loss to regional groundwater, and the corrected streamflow for model simulations (annual corrected discharge Q_{corr} factor)

Year	*P* (mm)	PET (mm)	Q_{obs} (mm)	Water loss	Annual Q_{corr} factor	Q_{corr} (mm)
2016	4542	555	1773	49%	2.25	3987
2017	5466	603	1947	53%	2.50	4863
2018	6146	636	1747	61%	3.15	5510
2019	4314	653	918	64%	3.99	3661

$$\mathrm{KGE} = 1 - \sqrt{(1-r)^2 + (1-\gamma)^2 + (1-\beta)^2} \quad (4)$$

The objective function (KGE) was minimized for streamflow and stream deuterium by comparing measured values with those simulated from the TAM. We retained the best 500 parameter combinations, that is, those with the smallest Euclidian distance to an optimum in the two-dimensional criteria space of KGE for discharge and KGE for stream deuterium simulations of the three-year and the single-year calibration periods (2017, 2018 and 2019). The mean KGE of these 500 model runs for each calibration period and associated standard deviation (SD) is provided in Table 5 and used for visualizing the 90% uncertainty bounds. The resulting Pareto fronts and simulation envelopes serve as uncertainty indicators for model simulations. The parameter distributions from the calibration periods were compared to qualitatively assess parameter sensitivity and variability. Additionally, the parameter sets derived from the three-year calibration period (2017–2019) was used to simulate the streamflow and isotope response for 2016 for model validation.

3.3.1 | Water flux age tracking

Water ages were estimated with a flux tracking approach that requires each precipitation event to be tagged with a time stamp. Depending on the mixing and flow processes, water can stay in storage before contributing to streamflow, thereby increasing its age. We calculated and analysed the streamflow flux ages for the whole period (2016–2019) and single years, using the best 500 parameter sets from the calibration with the three-year period (2017–2019). The results were used to derive water flux age distributions (cf. Birkel et al., 2015; Hrachowitz et al., 2013):

$$P_{F,Q}(t_j - t_i, t_j) = \sum_{n=1}^{N} P_{F,Q_n}(t_j - t_i, t_j)\,\frac{Q_n(t_j)}{Q(t_j)} \quad (5)$$

with $P_{F,Q}$ representing the distribution of water age of all contributing fluxes Q_n to the total discharge Q, with t_j being the time of exit at the catchment outlet and t_i the time of entry with P.

3.4 | Ensemble hydrograph separation

We compared the GM and TAM approaches to estimate water ages and TTs with the EHS approach presented by Kirchner (2019). Matching tracer input–output records, the EHS allows to derive TTDs and young water fractions in streamflow, defined as the fraction of runoff with transit times of less than a threshold age (usually 0.2 years). We used the R scripts from Kirchner, and Knapp et al. (2020) on the daily isotope series of 2016 and the weekly series of 2017. Due to the increasing loss of precision with coarse sampling frequency, we did not simulate the data from 2018 and 2019. The TTD and young water fraction were estimated assuming an interception storage of 1 mm of rainfall and no outliers in our data.

4 | RESULTS

4.1 | Hydrometeorology and stable isotope characteristics

Measured streamflow amounts ranged from 918 mm/a in the drier year 2019 to 1947 mm/a in the wetter year 2017 (Table 3), while

TABLE 5 Comparison of model performance statistics (KGE, SD_{KGE} for stream deuterium ratio simulations) for the retained best-fit parameters and resulting mean age estimates of the gamma model (GM) with corresponding mean transit time (MTT) compared to the tracer-aided model (TAM) with mean flux age. The three-years calibration period from 2017 to 2019 was compared to the single years used for calibration, as well as the evaluation year 2016

Model	GM	TAM
Period	**MTT (d)**	**Flux age (d)**
2016–2019	**87**	**49**
SD_{age}	0.0	44
KGE	0.88	0.91
SD_{KGE}	0.00	0.02
2016	**96**	**39**
SD_{age}	0.0	28
KGE	0.89	0.53[a]
SD_{KGE}	0.00	0.05[a]
2017	**83**	**40**
SD_{age}	1	43
KGE	0.95	0.94
SD_{KGE}	0.00	0.02
2018	**95**	**46**
SD_{age}	0.2	43
KGE	0.93	0.93
SD_{KGE}	0.00	0.03
2019	**289**	**71**
SD_{age}	0.6	63
KGE	0.89	0.90
SD_{KGE}	0.00	0.01

[a]Validation: Performance of 2017–2019 calibration simulating 2016 data.

mean annual ET ranged from 555 mm/a to 653 mm/a similar to ET from other cloud forests in the country (Dehaspe et al., 2018). The measured annual water balance indicates a regional loss of water to deeper groundwater that does not contribute to local streamflow since the measured inputs (P) were much higher than the measured outputs (sum of Q and ET, Table 3).

The water balance mismatch was up to 64% of annual precipitation, exceeding by far any measurement uncertainty (i.e., Figure S3). Even an exaggerated underestimation of ET by 100% cannot explain a loss of over 2000 mm/a of water. Interestingly, similar volumes of water surplus were measured downstream of our study site at La Selva Biological Station located within the Caribbean plains (Genereux et al., 2013; Wiegand & Schwendenmann, 2013). The missing water volumes were therefore corrected annually for modelling (correction factor: $\frac{P-ET}{Q}$), yielding a new corrected discharge Q_{corr} (Table 4). We corrected the water balance for modelling rather than parameterizing a water loss to constrain parameter uncertainty and to avoid unrealistic parameter estimations.

The almost constant cloud cover over the hilltops limits the energy input from irradiation, which together with the constantly high relative humidity (close to saturation) constrains the evapotranspiration loss to around 10% of the total rain input (Table 4, Figure S2C).

The calculated LMWL, based on daily rainwater samples, plots slightly above the GMWL in the dual isotope plot (Figure 3) and is best described by $\delta^2H = 8.26\ \delta^{18}O + 14.75$ ($r^2 = 0.98$, $n = 906$). The regression lines for both surface and soil water isotopes were almost identical to the LMWL (Figure 3), denoting a strong and recent meteoric origin with little to no evidence for evaporative fractionation. Identical mean isotope values for rainfall and streamflow indicate an isotopic mass equilibrium (Table 3). The isotope variability decreased from rainfall to soil water and groundwater with streamflow isotope ranges being enclosed by soil and groundwater isotopes. However, the variability of streamflow isotopes showed little damping compared to rainfall input indicating a quickly responding system with limited mixing.

The rainfall input and the slightly damped but quickly changing streamflow isotope ratios for deuterium showed a bimodal pattern (W-mode type) every year, which reflects the rainfall seasonality (Figure 4). The drier months (January–February), dominated by north-easterly trade winds, and the mid-summer drought are characterized by isotopically enriched rainfall across the region. Two pulses during the wet seasons (May and October/November) bring depleted precipitation into the system (Sánchez-Murillo & Birkel, 2016; Sánchez-Murillo, Romero-Esquivel, et al., 2019).

The hydrological year 2016 was one of the strongest El Niño years on record and started with a strong dry season as a carry-over effect of the drought from the end of 2015 (Climate Prediction Center Internet Team, 2020); the category 3 hurricane "Otto" caused a large isotopic depletion in November 2016 (Sánchez-Murillo, Durán-Quesada, et al., 2019). Similarly, the tropical storm Nate in October 2017 brought the most depleted rainfall of the whole 4 years period. In addition, 2018 was a typical La Niña year, resulting in an above average humid year but with no specific storms. The largest peak flow event during the entire sampling period occurred in January 2018 and was associated with prolonged intense rainfall from a cold front of 1111 mm during that month. In contrast, 2019 was again a drier but weak El Niño year.

4.2 | Model simulations, parameter uncertainty and independent evaluation

The GM reasonably simulated the streamflow isotope ratios with mean values (±SD) for $\alpha = 0.51$ (±0.00), $\beta = 170$ (±0.1 days; and a KGE of about 0.88) matching the peak events as well as recession periods (Figure 4). The KGE values of the GM indicated an overall good model performance. The model fit was slightly better for the wetter and more variable years 2017 and 2018 (KGE > 0.93).

The Pareto fronts (Figure 5) evaluating streamflow and isotope performance of the 500 best fitting TAM simulations show the two-dimensional space of the objective functions (KGE Q and KGE δ^2H) for calibration of the three-year period (2017–2019), and the individual years (2017, 2018, 2019). The single year calibrations showed little difference in model performance compared to the three-years simulation, with overall high KGEs >0.90 for isotope simulations and >0.75 for discharge. The Pareto front for 2018 showed the most distinctive inflection point, indicating a model performance close to optimal values with virtually no trade-off between discharge or isotope performance. The driest year 2019 was characterized by the smallest isotope input variability and also the most modest model performance compared to the other years. The three-years calibration yielded a reasonable performance balancing the individually calibrated years and was used for the simulation of the entire data series and validation in 2016 (Figure 5).

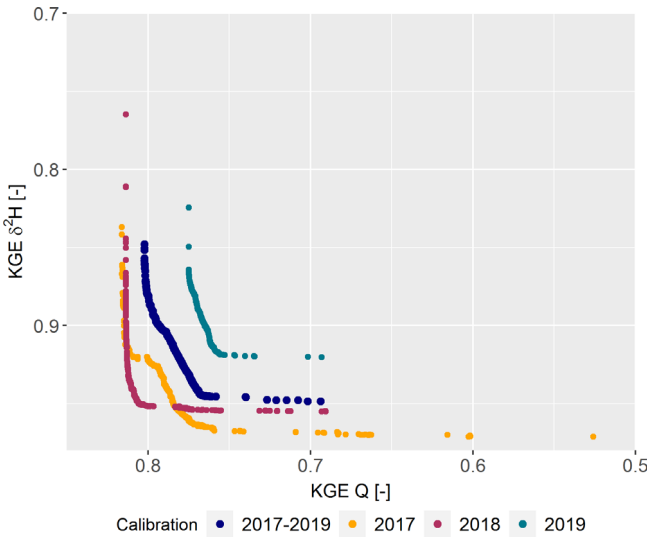

FIGURE 5 Pareto fronts of the retained 500 best-fitting parameter sets in the two-dimensional criteria space of discharge (KGE Q) and stream isotope KGE (KGE δ^2H) for the complete calibration period and individual calibration years

The posterior distribution of the eight 500 best-fit parameters for each of the calibrations is shown in Figure 6. The posterior distribution indicates how constrained a parameter range is after calibration and is a proxy for parameter identifiability. The most constrained parameters were *a*, *b*, *c* and α for the five-parameter rainfall-runoff model and the upper passive mixing volume MV_{up} (Figure 6a,b,d,e,f) for tracer transport (compare Table 2). The riparian area mixing volume MV_{rip} (Figure 6g) was identifiable but differed for the individual calibrations. The groundwater-related parameters *R* and MV_{GW} (Figure 6c,h), which are responsible for contributing older water, were less constrained.

The temporal pattern of discharge simulations at the catchment outlet (Figure 7c,f) followed these of rainfall (Figure 7a), indicating a quick system response to inputs. The TAM simulations matched the seasonal variability as well as the peaks and minima of the measured discharge (Figure 7c) and the isotope ratio for deuterium (Figure 7f) well for 2017 to 2019 (KGE = 0.91). The uncertainty bounds were relatively narrow due to the multi-objective optimization algorithm consistently converging towards a global minimum. Validating the calibration, the simulation of the 2016 data resulted in poorer but still reasonable model performance for stream deuterium (KGE = 0.53) capturing the observed seasonality (Figure 7f).

For soil water (Figure 7d), there was relatively fewer observations available, and we used it as an independent evaluation of internal model fluxes, which the model matched well with KGE > 0.59. The groundwater isotope measurements (Figure 7e) were too few to quantitively evaluate the model performance, but it is worth mentioning, that the model captured two of the three data points within the 90% interval. The independent evaluation of internal model states gives reason to assume that the model structure appropriately reflects the most dominant hydrological processes of the studied catchment.

The relative groundwater contribution to streamflow (baseflow index, BFI; Figure 7b), was 37% (±22%) of total discharge for the four-year period (2016: 42% (±25%); 2017: 36% (±22%); 2018: 35% (±19%); 2019: 35 (±22%). The relation of baseflow to surface runoff within the TAM highlights a near-surface dominated system of upper soil water flow paths that quickly converts rainfall with little mixing into streamflow (Figure 8).

We further examined the most prominent extreme events of the measurement period (Figure 8b–d). Hurricane Otto (November 2016, Figure 8b) with a daily rainfall up to 123 mm and tropical storm Nate with rainfall of more than 300 mm in 48 h (Figure 8c) caused large peak flows and significant surface flows (event average of 80%). The

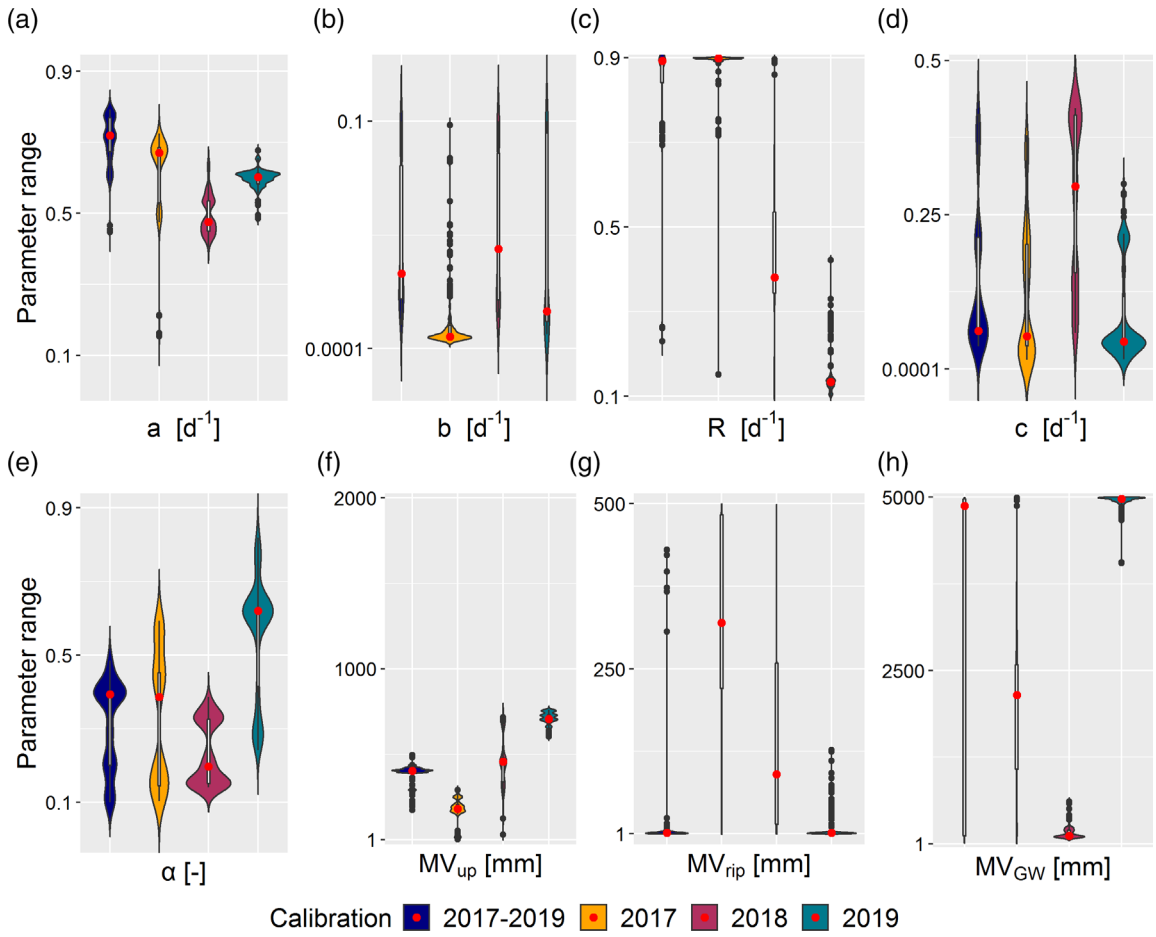

FIGURE 6 Posterior parameter distributions of the retained 500 best parameter sets of the different TAM calibrations visualized as violin plots. The shape of the violin plots depicts the frequency of the 500 parameter values, whereas the red dots are the medians for each parameter and calibration. The ordinate limits were set to the parameter interval for calibration (as presented in Table 2)

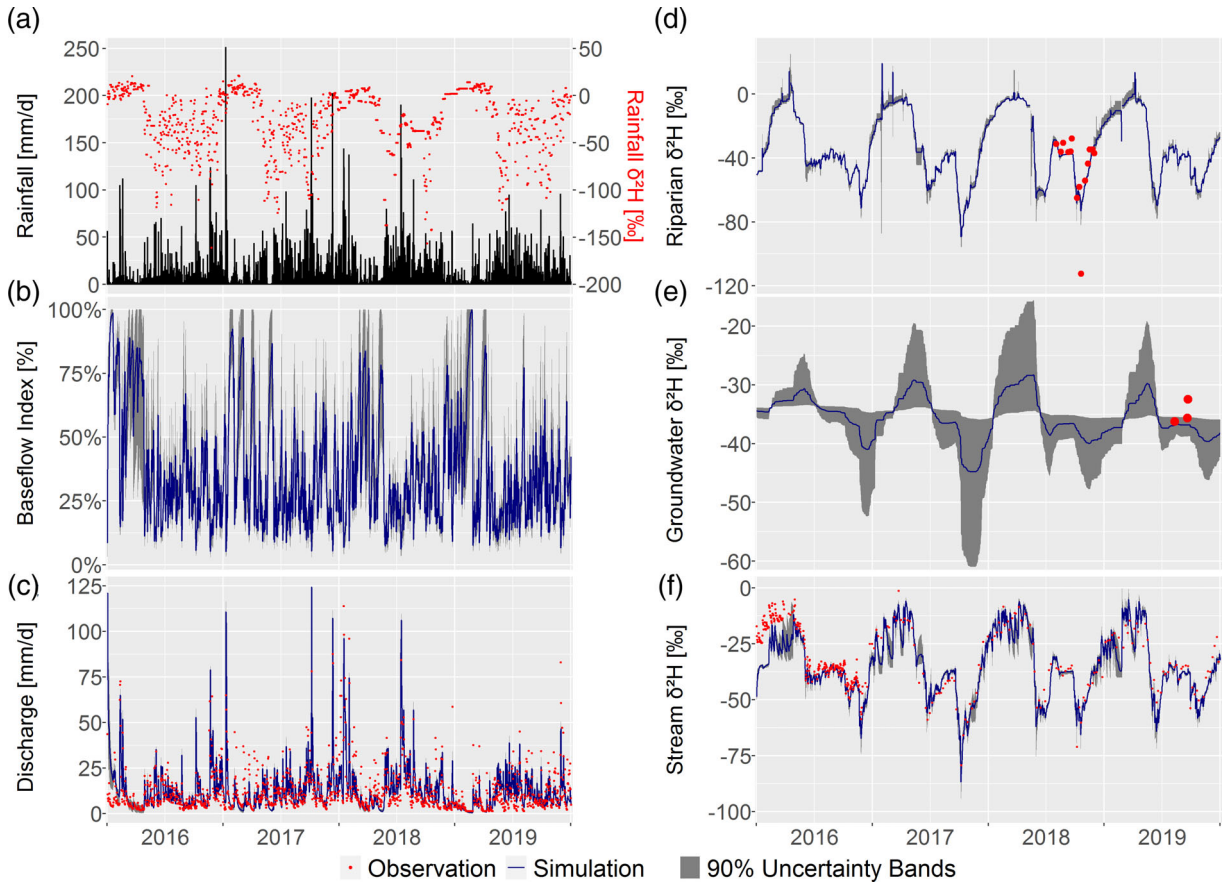

FIGURE 7 Tracer-aided model simulation: (a) model input data: Rainfall rates (black bars) with deuterium ratios in precipitation (red dots), (b) estimated base flow index, (c) the observed and simulated streamflow with 90% uncertainty bands, (d) simulated deuterium ratios from the riparian storage, (e) simulated groundwater storage and measured soil water/groundwater isotope ratio as an independent model evaluation and (f) simulated and observed streamflow isotope ratios. Model simulations are shown with a blue line, the grey shading represents the 90% uncertainty

water flux ages were in the order of a few days. The re-wetting event after a relatively dry period of about 1 week in 2019 with 100% groundwater contribution to streamflow (Figure 8d) was also simulated quite well by the model with an immediate response of near-surface runoff (KGE = 0.64 for 2019).

4.3 | Transit time, young water fraction and water flux age estimations

Figure 9 shows the simulated daily stream water flux ages together with discharge. The non-stationary nature of the daily average water flux ages was clearly reflected by the fluctuations between water that was a few days old during peak flow events and water ages up to a maximum of 1 year during drier periods in mid-2016 and the beginning of 2019. The mean annual water ages of the TAM ranged from 39 days in 2016 up to 71 days in 2019 (Table 5).

Table 5 shows a direct comparison of the annual MTT estimates of the GM with the mean flux ages of the TAM and associated standard deviations (SD_{age}), as well as model performance statistics (KGE, SD_{KGE} for streamflow deuterium simulations). The MTTs of the GM were slightly longer compared to the TAM but always shorter than 1 year (annual MTT = 9.5 months in 2019; Table 5). The concordance between the two models was greater for the wetter years with a lower estimated age and diverged for the drier 2019 with an MTT of 289 days of the GM compared to a flux age of 71 days of the TAM. The TAM calculated slightly younger ages for 2016 compared to the four-year average due to Hurricane Otto causing surface flow with short transit times. The shortest MTTs were simulated for 2017, a wet La Niña year influenced by the tropical storm Nate.

Figure 10 compares the different approaches to estimating water ages. They all agreed on the young water dominance of the study catchment with a young water fraction threshold of around 12 days. Moreover, the best-fit GM TTD approximated the EHS-derived TTD and Cumulative Distribution Function (CDF; Figure 10a,b). The TAM water age distribution cannot directly be compared to the GM and EHS TTDs but also indicated that most estimated water ages were below 2 months old.

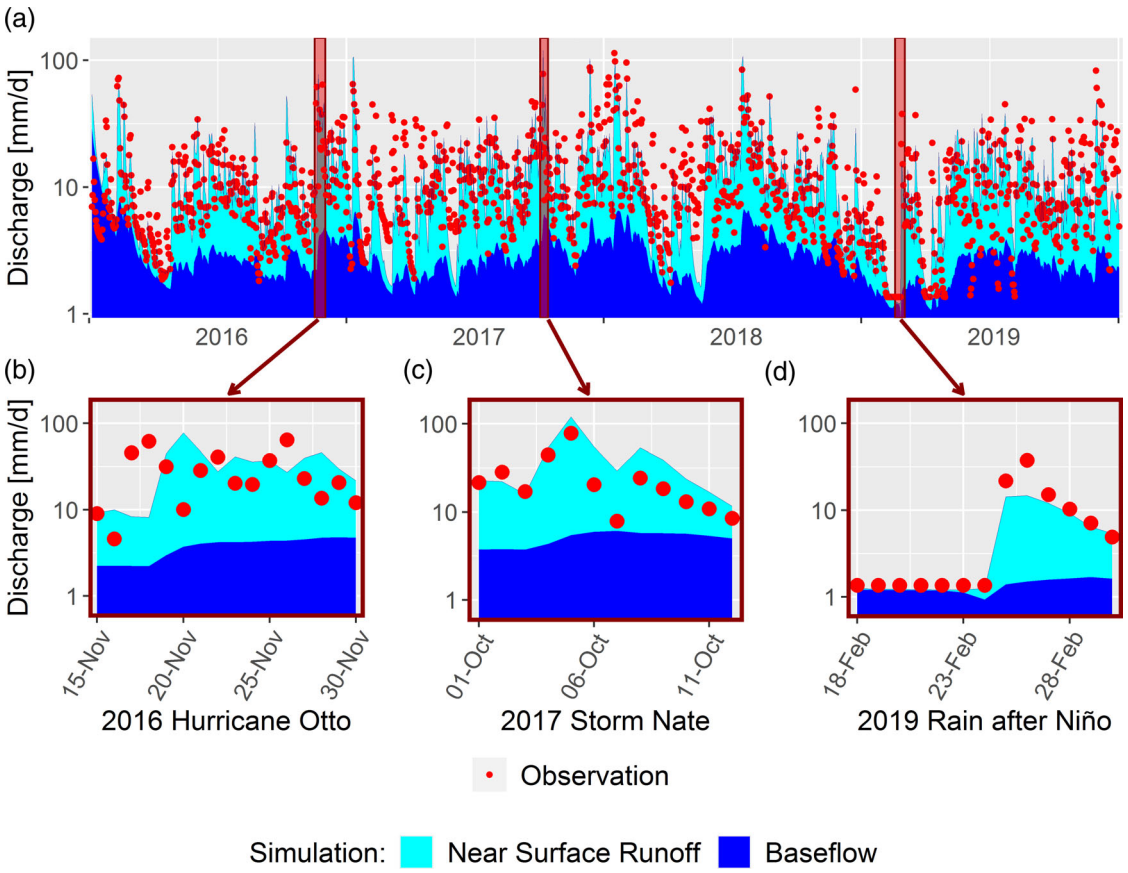

FIGURE 8 (a) Hydrograph separation into near surface runoff and baseflow by the TAM. (b–d) Three events are highlighted to show the streamflow response and BFI to different extreme rainfall or drought periods. Note that discharge is plotted on a log scale

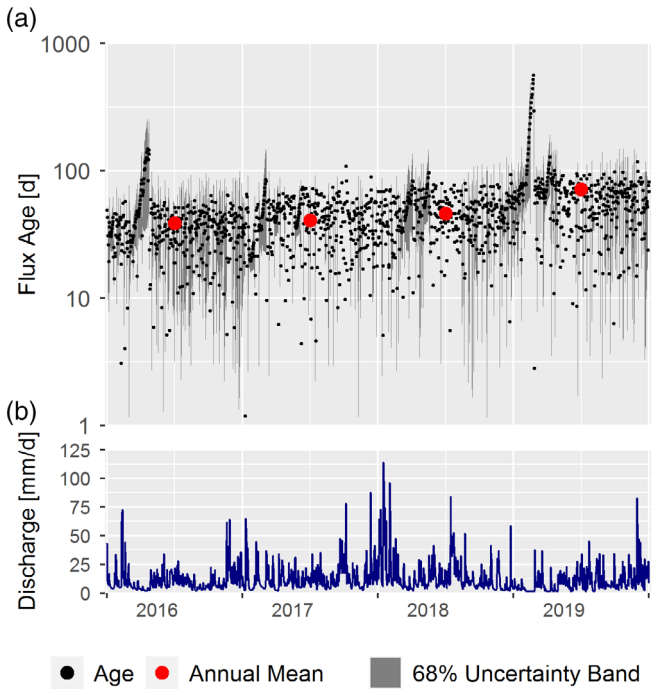

FIGURE 9 (a) Simulated daily streamwater flux age (log-scale) time series with annual mean values and (b) observed streamflow

5 | DISCUSSION

5.1 | Runoff generation and mixing in a very humid rainforest catchment

The average annual precipitation of approximately 5000 mm in our study area (Table 4) exceeds the country-wide average of about 3000 mm (Sánchez-Murillo et al., 2017). The measured average $\delta^{18}O$ values of rainfall correspond to those of the Caribbean domain of $-5.0 \pm 2.4‰$, where they are generally slightly more enriched than on the Pacific slope (Sánchez-Murillo, Esquivel-Hernández, Birkel, et al., 2020).

The weak damping effect of the isotope ratios in streamflow compared to rainfall (Table 3; Figure S4) indicated a rapid runoff generation with limited isotope mixing in soils and groundwater, similar and even more pronounced than for other catchments in Costa Rica (Birkel et al., 2021). Similarly to other case studies in headwater catchments of tropical areas (Goller et al., 2005), rainfall intensity and distribution is a major driver of the rapid streamflow response (Bonell et al., 1998, p. 367).

Surely, a daily model time step misses part of rainfall intensity variations and the rapid hourly streamflow response, but a simultaneous sub-daily rainfall-runoff and isotopic monitoring in the tropics and

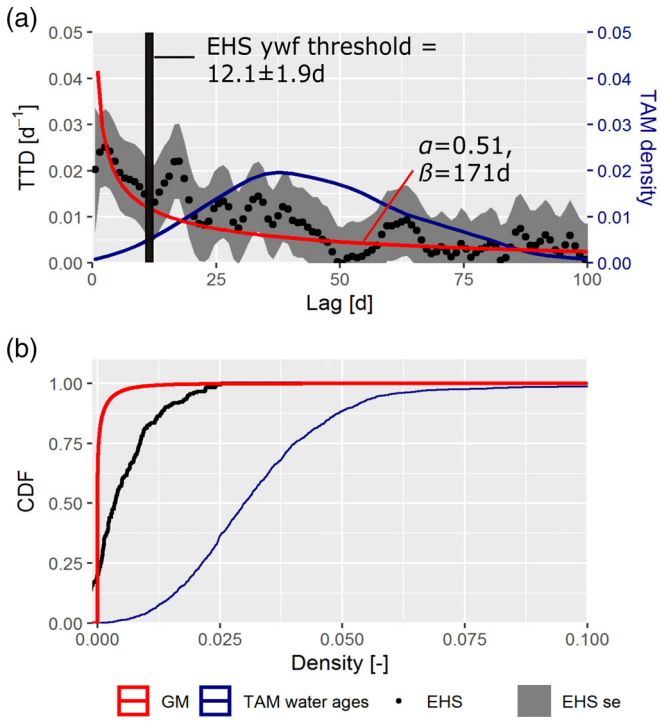

FIGURE 10 (a) The best-fit GM (gamma model) and ensemble hydrograph separation (EHS) derived transit time distributions (TTDs) are shown in comparison to the distribution of water ages from the tracer-aided model (TAM) with a black mark indicating the EHS-derived young water fraction threshold and (b) the cumulative distribution functions (CDFs) derived from the TTDs and TAM water age distribution

elsewhere is still a major challenge (von Freyberg et al., 2017). Nonetheless, the TAM identified quickly draining water from the upper soil water storage at the hillslopes directly into the saturated riparian zone (Sánchez-Murillo, Romero-Esquivel, et al., 2019). From there, mostly unmixed water (Figure 6f,g with low mixing volume parameters MV) rapidly contributes to streamflow, as reflected by high values (Figure 6a,e) of the linear rate coefficients *a* (Flow from hillslope to riparian area; Table 2) and the non-linear parameter α (flow from riparian area to stream; Table 2). The most likely runoff generation mechanism is saturation excess overland flow and near-surface stormflow. In fact, field observations during sampling campaigns confirmed the prevalence of swamp areas near the riparian zones. Hortonian overland flow can be excluded due to the measured high infiltration capacities of the humic top soil layer that exceed the highest observed rainfall intensities in contrast to other small-scale catchments in Latin America (Chaves et al., 2008; Zimmermann et al., 2012).

The comparison of different calibration periods and storage parameters showed that only the upper hillslope has a larger mixing volume (Figure 6f), but that water passes too fast likely via preferential flow pathways to noticeably dampen the isotope output variability. The variability in some storage parameters could be related to the rainfall volumes from the individual years (Figure 6f) with lower rainfalls and subsequently less storage resulting in more insensitive parameters particularly related to the more difficult to constrain older groundwater. Such behaviour of quick near-surface runoff generation was previously observed in other tropical catchments (Birkel et al., 2021) and in catchments with a different climate, such as in the Scottish Highlands (Soulsby et al., 2015). Yet, in the study of Soulsby et al. (2015) the observed and simulated catchment response was less quick with more mixed and older waters. Bonell et al. (1998) distinguished two types of rainfall-runoff and mixing behaviour: Low rainfall intensities lead to groundwater replacement in the sub-surface pathways and a "first-in-first-out" response. Instead, high precipitation rates short-circuit these pathways exceeding their capacity leading to a rapid response of event water in the stream: the "last-in-first-out" type of behaviour. Such quick responding systems vertically percolate water into deeper storage via preferential flow pathways.

In our case, however, the hydrograph separation (Figure 8) indicated a constant but small contribution of water from a deeper substrate to the perennial stream (average BFI of 37% ± 22%; Figure 7b). The water balance showed a loss of water from our system (Table 4) indicating that a fraction of vertical water fluxes percolates into the highly fractured volcanic bedrock, and thus cannot be measured as streamflow at the catchment outlet. Evidence for re-emerging regional groundwater were found in the floodplains downstream of the study site using age dating tracers (Genereux et al., 2013) and modelling (Osburn et al., 2018; Zanon et al., 2014). Irrigation experiments as by Graham et al. (2010) could empirically quantify this seepage.

The low BFIs support the notion of a saturation excess surface runoff and shallow interflow dominated system (Sánchez-Murillo, Romero-Esquivel, et al., 2019). Interestingly, the BFIs in our study area were also much lower than observed for other catchments in Costa Rica (Birkel et al., 2012; Westerberg & Birkel, 2015) and other tropical catchments (Beck et al., 2013; Peña-Arancibia et al., 2010) which are commonly characterized by high groundwater contributions to total streamflow. Even in other fast responding catchments in Costa Rica, the flashy response in streamflow after storm events is characterized by mixing and dampening effects from available deeper soil and groundwater (Dehaspe et al., 2018).

Therefore, our study site is a pristine catchment (Klaus & McDonnell, 2013) in the central American tropics that deviates from the old water paradox (Barthold & Woods, 2015; Sidle et al., 2000), that is, the rapid mobilization of previously stored "old" water via subsurface flow paths during storm events (Muñoz-Villers & McDonnell, 2012), resulting in strongly damped tracer output composition (Kirchner, 2003). Due to the young water dominance, short TTs and low groundwater contribution to streamflow, we, therefore, rejected our previously formulated working hypothesis.

5.2 | The role of water ages as an indicator of catchment functioning

The GM (KGE > 0.88) and TAM (KGE > 0.91) models performed much better than other applications with similarly measured daily isotope datasets and conceptual models in Costa Rica (Birkel & Soulsby, 2016). The independent model evaluation against soil and

groundwater isotope measurements (Figure 7d,e) further increased confidence in the findings (Birkel et al., 2014; Kuppel et al., 2018). Furthermore, the model split sample test showed relative robustness for different calibration periods and an overall good performance of streamflow and stream isotope simulations (Figure 5). Surely, uncertainties in model results due to uncertain input data and model assumptions cannot be neglected (see section 5.1), but seem to be less prominent for the small Quebrada Grande catchment compared to other modelling studies in the tropics (Collischonn et al., 2008; Rafiei Emam et al., 2018; Westerberg et al., 2014; Westerberg & Birkel, 2015). The water flux age tracking, based on streamflow and isotope simulations, benefitted from the overall low TAM uncertainties. Despite some general doubts concerning the underestimation of MTTs and aggregation errors with TAM (DeWalle et al., 1997; Kirchner, 2016a), for our catchment, characterized by relatively short TTs and young water fluxes, the approach has the potential to provide a first reasonable approximation of hydraulically active and total catchment-scale storage.

The MTT and flux age estimates are mathematically not equivalent (Hrachowitz et al., 2013). The MTT is based on damped tracer compositions and flux ages are based on the tagged model input–output time lag. Yet, both estimates reflect climate patterns of drier and wetter years influenced by extreme events (Hrachowitz et al., 2011) and the shorter TTs and flux ages reflect the dominance of saturation excess surface flow and near-surface runoff contributing younger and unmixed waters to streamflow. The longest annual MTT of 9.5 months (2019) of the GM resulted from slightly lower input–output isotope variability. Similarly, for the TAM, during drier periods when discharge was low, it was fed by older waters resulting in slightly older streamflow (Figure 8d). The TAM flux age calculation overcomes the weaknesses of the steady-state assumption and a priori definition of a TTD of the simpler GM (Hrachowitz et al., 2013) but carries the risk of non-unique solutions because of more calibrated parameters (8 TAM versus 2 GM). In contrast, the GM estimated short MTTs resulted from an almost globally comparable alpha parameter of 0.5 (Godsey et al., 2010). Consequently, the eight calibrated TAM parameters cause a wider posterior parameter range in comparison to the GM, hence the TAM SD_{age} of flux ages resulting from the retained parameters after calibration is larger. Nonetheless, the comparable MTT and water flux age results of the two independent models increase the confidence in viable and trustworthy model results.

Jasechko et al. (2016) have concluded in a global study that most rivers exhibit a fairly high proportion of young water, that is, less than 3 months old. The annual water flux ages, derived by the TAM, can therefore be classified as young streamflow. This was corroborated with the EHS-derived TTD and young water fraction threshold of 12.1 ± 1.9 days following the approach of Kirchner (2019). The EHS-derived TTD even approximated the best-fit GM TTD (Figure 10). Such young water estimates support previous results for a single year (2017) with an MTT of around 96 days that used a simple exponential model (Sánchez-Murillo, Romero-Esquivel, et al., 2019). Our results are also in line with other studies (Ala-aho et al., 2017; Hrachowitz et al., 2013; Piovano et al., 2019; Remondi et al., 2018) supporting the detected non-stationary nature of water ages depending on antecedent wetness and amount of water in storage (Harman, 2015).

Young streamflow usually results from short resident times in the subsurface and is composed of a minimal groundwater portion (Jasechko et al., 2016). Therefore, this catchment is an extremely fast responding system and only comparable to steep, wet catchments with thin soils on an impermeable bedrock such as in western Scotland (Hrachowitz, Soulsby, Tetzlaff, Dawson, & Malcolm, 2009). Furthermore, there is no measured geochemical evidence (e.g., silica, cations) in streamflow for the fraction of deeper groundwater of an unknown age. Stream mean annual EC is 7.79 ± 7.04 μS/cm, which indicates short water-rock-soil contact time. Our water ages and MTT estimates are also quite short for Costa Rican conditions as previous works in other steep rainforest catchments showed fast responding systems, but with more sub-surface mixing involved and therefore slightly longer MTTs and older water age estimates of around one-year (Birkel & Soulsby, 2016; Correa et al., 2020).

6 | CONCLUSIONS

This study shows how long-term hydrometric and isotopic data sets can be used with different model approaches and methods to simulate streamflow and isotope ratios to obtain water age estimates. The simple GM, together with the hydrometeorological understanding of the rainfall-runoff transformation, already resulted in broad insights into the hydrological processes of our remote tropical catchment. The relatively parsimonious tracer-aided rainfall-runoff model (TAM) further enhanced these findings by the simultaneous simulation of streamflow and stream isotope ratios, because it distinguishes the total runoff into base flow and surface runoff and provides water flux age estimates. The TAM was satisfactorily evaluated for a respective single year using observed groundwater and soil water isotope data, increasing the confidence in simulations.

The TAM demonstrated the non-stationarity of catchment water ages with water of a few days old in streamflow during storm events and slightly older waters up to 1 year old during rare week-long rain-free periods. The stationary GM resulted in variable transit times depending on the climatic conditions if tested on individual years. Both models seemed to agree on waters younger than 3 months for over 75% of the measurement period from 2016 to 2019. The latter was further corroborated by EHS-derived young water fractions and a TTD that approximates those of the best-fit GM derived TTDs. Despite perennial flows in the Quebrada Grande, the BFI (<37%) was much lower than in other tropical catchments resulting in a line of evidence that suggested young water streamflow generation in this pristine, forested system. The combination of these hydrological processes resulted in an extremely fast responding system that is likely more vulnerable to climatic variability and forecasted increase of weather extremes than other systems with a higher water storage capacity. Young water ages revealed by the three different methods provided insights into solute transport.

The comparison of different calibration periods and storage parameters showed that only the upper hillslope provides notable water storage for mixing, but that water passes too fast to significantly affect solute transport, as indicated by the measured isotope variability. It could also be concluded that groundwater recharge potentially occurs throughout longer rainy periods rather than extreme events, and that a significant volume of rainfall input contributes to a regional groundwater flow invisible at the catchment outlet.

Despite some limitations of tracer simulations and inevitable model uncertainties, the combined analysis of hydrometric and isotopic data integrated into hydrological models helps to understand the dominant hydrological processes in the quest for a more complete picture of water quantity and quality dynamics in the tropics.

ACKNOWLEDGEMENTS

This study was partially funded by multiple institutions and grants. Support from the International Atomic Energy Agency (IAEA) grants COS/7/005 and RC-19747 (CRP-F31004 and CRP-F31005) is recognized. Funding from the Research Office of Universidad Nacional (Heredia, Costa Rica) and Empresa de Servicios Públicos de Heredia (ESPH) was crucial for conducting sampling campaigns and maintaining continuous hydrometric measurements. C.B. would like to thank the Leverhulme Trust for partly covering research time (ISOLAND project: RPG-2018-375).

DATA AVAILABILITY STATEMENT

The data that support the findings of this study are openly available in hydroshare at Sánchez-Murillo, R., L. Mayer-Anhalt, C. Birkel, S. Schulz (2021). Daily hidrometric and stable isotope database at Quebrada Grande rainforest catchment, Costa Rica, HydroShare, http://www.hydroshare.org/resource/0cdad4c81d2545408e43867d48fedfe9; DOI: 10.4211/hs.0cdad4c81d2545408e43867d48fedfe9.

ORCID

Leia Mayer-Anhalt https://orcid.org/0000-0002-3546-6164
Christian Birkel https://orcid.org/0000-0002-6792-852X
Ricardo Sánchez-Murillo https://orcid.org/0000-0001-8721-8093
Stephan Schulz https://orcid.org/0000-0001-7060-7690

REFERENCES

Aguilar E., Peterson T. C., Obando P. R., Frutos R., Retana J. A., Solera M., Soley J., García I. G., Araujo R. M., Santos A. R., Valle V. E., Brunet M., Aguilar L., Álvarez L., Bautista M., Castañón C., Herrera L., Ruano E., Sinay J. J., Mayorga R. (2005). Changes in precipitation and temperature extremes in Central America and northern South America, 1961–2003. *Journal of Geophysical Research*, *110*(D23), 1–15. https://doi.org/10.1029/2005jd006119

Ala-aho P., Tetzlaff D., McNamara J. P., Laudon H., Soulsby C. (2017). Using isotopes to constrain water flux and age estimates in snow-influenced catchments using the STARR (Spatially distributed Tracer-Aided Rainfall–Runoff) model. *Hydrology and Earth System Sciences*, *21*(10), 5089–5110. https://doi.org/10.5194/hess-21-5089-2017

Allen, R. G., Pereira, L. S., Raes, D., & Smith, M. (1998). *Crop evapotranspiration: Guidelines for computing crop water requirements* (p. 300). Food and Agriculture Organization of the United Nations. Available from: http://www.kimberly.uidaho.edu/water/fao56/fao56.pdf.

Allen, S. T., Keim, R. F., Barnard, H. R., McDonnell, J. J., & Renée, B. J. (2017). The role of stable isotopes in understanding rainfall interception processes: A review. *WIREs Water*, *4*(1), 1–17. https://doi.org/10.1002/wat2.1187

Aparecido, L. M. T., Miller, G. R., Cahill, A. T., & Moore, G. W. (2016). Comparison of tree transpiration under wet and dry canopy conditions in a Costa Rican premontane tropical forest. *Hydrological Processes*, *30*(26), 5000–5011. https://doi.org/10.1002/hyp.10960

Mullen K., Ardia D., Gil D., Windover D., Cline J. (2011). DEoptim: AnRPackage for Global Optimization by Differential Evolution. *Journal of Statistical Software*, *40*(6), https://doi.org/10.18637/jss.v040.i06

Barthold, F. K., & Woods, R. A. (2015). Stormflow generation: A meta-analysis of field evidence from small, forested catchments. *Water Resources Research*, *51*(5), 3730–3753. https://doi.org/10.1002/2014WR016221

Beck, H. E., Van Dijk, A. I. J. M., Miralles, D. G., De Jeu, R. A. M., Bruijnzeel, L. A., McVicar, T. R., & Schellekens, J. (2013). Global patterns in base flow index and recession based on streamflow observations from 3394 catchments. *Water Resources Research*, *49*(12), 7843–7863. https://doi.org/10.1002/2013WR013918

Berman, E. S. F., Levin, N. E., Landais, A., Li, S., & Owano, T. (2013). Measurement of δ18O, δ17O, and 17O-excess in water by off-axis integrated cavity output spectroscopy and isotope ratio mass spectrometry. *Analytical Chemistry*, *85*(21), 10392–10398. https://doi.org/10.1021/ac402366t

Bierkens, M. F. P., & van den Hurk, B. J. J. M. (2007). Groundwater convergence as a possible mechanism for multi-year persistence in rainfall. *Geophysical Research Letters*, *34*(2), 1–5. https://doi.org/10.1029/2006GL028396

Birkel C., Correa Barahona A., Duvert C., Granados Bolaños S., Chavarría Palma A., Durán Quesada A. M., Sánchez Murillo R., Biester H. (2021). End member and Bayesian mixing models consistently indicate near-surface flowpath dominance in a pristine humid tropical rainforest. *Hydrological Processes*, *35*, (4), 1–13. https://doi.org/10.1002/hyp.14153

Birkel, C., & Soulsby, C. (2015). Advancing tracer-aided rainfall-runoff modelling: A review of progress, problems and unrealised potential. *Hydrological Processes*, *29*(25), 5227–5240. https://doi.org/10.1002/hyp.10594

Birkel, C., & Soulsby, C. (2016). Linking tracers, water age and conceptual models to identify dominant runoff processes in a sparsely monitored humid tropical catchment. *Hydrological Processes*, *30*(24), 4477–4493. https://doi.org/10.1002/hyp.10941

Birkel, C., Soulsby, C., & Tetzlaff, D. (2012). Modelling the impacts of land-cover change on streamflow dynamics of a tropical rainforest headwater catchment. *Hydrological Sciences Journal*, *57*(8), 1543–1561. https://doi.org/10.1080/02626667.2012.728707

Birkel, C., Soulsby, C., & Tetzlaff, D. (2014). Developing a consistent process-based conceptualization of catchment functioning using measurements of internal state variables. *Water Resources Research*, *50*(4), 3481–3501. https://doi.org/10.1002/2013WR014925

Birkel, C., Soulsby, C., & Tetzlaff, D. (2015). Conceptual modelling to assess how the interplay of hydrological connectivity, catchment storage and tracer dynamics controls nonstationary water age estimates. *Hydrological Processes*, *29*(January), 2956–2969. https://doi.org/10.1002/hyp.10414

Bonal, D., Burban, B., Stahl, C., Wagner, F., & Hérault, B. (2016). The response of tropical rainforests to drought—Lessons from recent research and future prospects. *Annals of Forest Science*, *73*(1), 27–44. https://doi.org/10.1007/s13595-015-0522-5

Bonell, M., Barnes, C. J., Grant, C. R., Howard, A., & Burns, J. (1998). *High rainfall, response-dominated catchments: A comparative study of experiments in tropical northeast Queensland with temperate New Zealand*. Elsevier B.V. https://doi.org/10.1016/b978-0-444-81546-0.50018-5

Bony, S., Risi, C., & Vimeux, F. (2008). Influence of convective processes on the isotopic composition (δ18O and δD) of precipitation and water vapor in the tropics: 1. Radiative-convective equilibrium and Tropical Ocean-Global Atmosphere-Coupled Ocean-Atmosphere Response Experiment (TOGA-COARE). *Journal of Geophysical Research Atmospheres*, *113*(19), 1–21. https://doi.org/10.1029/2008JD009942

Bouroncle, C., Imbach, P., Rodríguez-Sánchez, B., Medellín, C., Martinez-Valle, A., & Läderach, P. (2017). Mapping climate change adaptive capacity and vulnerability of smallholder agricultural livelihoods in Central America: Ranking and descriptive approaches to support adaptation strategies. *Climatic Change*, *141*(1), 123–137. https://doi.org/10.1007/s10584-016-1792-0

Bowen, G. J. (2008). Spatial analysis of the intra-annual variation of precipitation isotope ratios and its climatological corollaries. *Journal of Geophysical Research Atmospheres*, *113*(5), 1–10. https://doi.org/10.1029/2007JD009295

Brujinzeel, L. A. (2001). Hydrology of tropical montane cloud forests: A Reassessment. *Land Use and Water Resources Research*, *1*, 1–15.

Chaves, J., Neill, C., Germer, S., Neto, S. G., Krusche, A., & Elsenbeer, H. (2008). Land management impacts on runoff sources in small Amazon watersheds. *Hydrological Processes*, *22*(12), 1766–1775. https://doi.org/10.1002/hyp.6803

Climate Prediction Center Internet Team. (2020). *Cold & warm episodes by season—National Weather Prediction*. Service, NOAA/National Weather Prediction, National Centers for Environmental Center, Climate Prediction Court, 5830 University Research. https://origin.cpc.ncep.noaa.gov/products/analysis_monitoring/ensostuff/ONI_v5.php

Collischonn, B., Collischonn, W., & Tucci, C. E. M. (2008). Daily hydrological modeling in the Amazon basin using TRMM rainfall estimates. *Journal of Hydrology*, *360*(1–4), 207–216. https://doi.org/10.1016/j.jhydrol.2008.07.032

Correa, A., Birkel, C., Gutierrez, J., Dehaspe, J., Durán-Quesada, A. M., Soulsby, C., & Sánchez-Murillo, R. (2020). Modelling non-stationary water ages in a tropical rainforest: A preliminary spatially distributed assessment. *Hydrological Processes*, *34*(25), 4776–4793. https://doi.org/10.1002/hyp.13925

Deb, K., Member, A., Pratap, A., Agarwal, S., & Meyarivan, T. (2002). A fast and elitist multiobjective genetic algorithm. *IEEE Transactions On Evolutionary Computation*, *6*(2), 182–197.

Dehaspe, J., Birkel, C., Tetzlaff, D., Sánchez-Murillo, R., Durán-Quesada, A. M., & Soulsby, C. (2018). Spatially distributed tracer-aided modelling to explore water and isotope transport, storage and mixing in a pristine, humid tropical catchment. *Hydrological Processes*, *32*(21), 3206–3224. https://doi.org/10.1002/hyp.13258

Delavau, C. J., Stadnyk, T., & Holmes, T. (2017). Examining the impacts of precipitation isotope input (δ 18 O ppt) on distributed, tracer-aided hydrological modelling. *Hydrology and Earth System Sciences*, *21*, 2595–2614. https://doi.org/10.5194/hess-21-2595-2017

DeWalle, D. R., Edwards, P. J., Swistock, B., Aravena, R., & Drimmie, R. J. (1997). Seasonal isotope hydrology of three appalachian forest catchments. *Hydrological Processes*, *11*(15), 1895–1906.

Durán-Quesada, A. M., Sorí, R., Ordoñez, P., & Gimeno, L. (2020). Climate perspectives in the Intra-Americas seas. *Atmosphere*, *11*(9), 1–32. https://doi.org/10.3390/ATMOS11090959

Esquivel-Hernández, G., Sánchez-Murillo, R., Birkel, C., & Boll, J. (2018). Climate and water conflicts coevolution from tropical development and hydro-climatic perspectives: A case study of Costa Rica. *Journal of the American Water Resources Association*, *54*(2), 451–470. https://doi.org/10.1111/1752-1688.12617

Genereux, D. P., Nagy, L. A., Osburn, C. L., & Oberbauer, S. F. (2013). A connection to deep groundwater alters ecosystem carbon fluxes and budgets: Example from a Costa Rican rainforest. *Geophysical Research Letters*, *40*(10), 2066–2070. https://doi.org/10.1002/grl.50423

Giorgi, F. (2006). Climate change hot-spots. *Geophysical Research Letters*, *33*(8), 1–4. https://doi.org/10.1029/2006GL025734

Godsey, S. E., Aas, W., Clair, T. A., de Wit, H. A., Fernandez, I. J., Kahl, J. S., … Kirchner, J. W. (2010). Generality of fractal 1/f scaling in catchment tracer time series, and its implications for catchment travel time distributions. *Hydrological Processes*, *24*(12), 1660–1671. https://doi.org/10.1002/hyp.7677

Goller, R., Wilcke, W., Leng, M. J., Tobschall, H. J., Wagner, K., Valarezo, C., & Zech, W. (2005). Tracing water paths through small catchments under a tropical montane rain forest in south Ecuador by an oxygen isotope approach. *Journal of Hydrology*, *308*(1–4), 67–80. https://doi.org/10.1016/j.jhydrol.2004.10.022

Gonzalez, J., Georgescu, M., Lemos, M., Hosannah, N., & Niyogi, D. (2017). Climate change's pulse is in Central America and the Caribbean. *Eos Transactions American Geophysical Union*, *98*. 1–7. https://doi.org/10.1029/2017EO071975

Graham, C. B., Van Verseveld, W., Barnard, H. R., & McDonnell, J. J. (2010). Estimating the deep seepage component of the hillslope and catchment water balance within a measurement uncertainty framework. *Hydrological Processes*, *24*(25), 3631–3647. https://doi.org/10.1002/hyp.7788

Gröning, M., Lutz, H. O., Roller-Lutz, Z., Kralik, M., Gourcy, L., & Pöltenstein, L. (2012). A simple rain collector preventing water re-evaporation dedicated for δ 18O and δ 2H analysis of cumulative precipitation samples. *Journal of Hydrology*, *448–449*, 195–200. https://doi.org/10.1016/j.jhydrol.2012.04.041

Gupta, H. V., Kling, H., Yilmaz, K. K., & Martinez, G. F. (2009). Decomposition of the mean squared error and NSE performance criteria: Implications for improving hydrological modelling. *Journal of Hydrology*, *377*(1–2), 80–91. https://doi.org/10.1016/j.jhydrol.2009.08.003

Hannah, L., Donatti, C. I., Harvey, C. A., Alfaro, E., Rodriguez, D. A., Bouroncle, C., … Solano, A. L. (2017). Regional modeling of climate change impacts on smallholder agriculture and ecosystems in Central America. *Climatic Change*, *141*(1), 29–45. https://doi.org/10.1007/s10584-016-1867-y

Harman, C. J. (2015). Time-variable transit time distributions and transport: Theory and application to storage-dependent transport of chloride in a watershed. *Water Resources Research*, *51*(1), 1–30. https://doi.org/10.1002/2014WR015707

Hrachowitz, M., Savenije, H., Bogaard, T. A., Tetzlaff, D., & Soulsby, C. (2013). What can flux tracking teach us about water age distribution patterns and their temporal dynamics? *Hydrology and Earth System Sciences*, *17*(2), 533–564. https://doi.org/10.5194/hess-17-533-2013

Hrachowitz, M., Soulsby, C., Tetzlaff, D., Dawson, J., & Malcolm, I. (2009). Regionalization of transit time estimates in montane catchments by integrating landscape controls. *Water Resources Research*, *45*(5), 1–17. https://doi.org/10.1029/2008WR007496

Hrachowitz, M., Soulsby, C., Tetzlaff, D., Dawson, J. J. C., Dunn, S. M., & Malcolm, I. A. (2009). Using long-term data sets to understand transit times in contrasting headwater catchments. *Journal of Hydrology*, *367*(3–4), 237–248. https://doi.org/10.1016/j.jhydrol.2009.01.001

Hrachowitz, M., Soulsby, C., Tetzlaff, D., & Malcolm, I. A. (2011). Sensitivity of mean transit time estimates to model conditioning and data availability. *Hydrological Processes*, *25*(6), 980–990. https://doi.org/10.1002/hyp.7922

IPCC. (2021). Climate Change 2021: The Physical Science Basis. Contribution of Working Group I to the Sixth Assessment Report of the Intergovernmental Panel on Climate Change. In: Masson-Delmotte, V., P. Zhai, A. Pirani, S.L. Connors, C. Péan, S. Berger, N. Caud, Y. Chen, L. Goldfarb, M.I. Gomis, M. Huang, K. Leitzell, E. Lonnoy, J.B.R. Matthews, T.K. Maycock, T. Waterfield, O. Yelekçi, R. Yu, and B. Zhou (eds.). Cambridge University Press. In Press.

Iraheta, A., Birkel, C., Benegas, L., Ríos, N., Sánchez-Murillo, R., & Beyer, M. (2021). A preliminary isotope-based evapotranspiration partitioning approach for tropical Costa Rica. *Ecohydrology*, *14*(5), e2297. https://doi.org/10.1002/eco.2297

Jasechko, S., Kirchner, J. W., Welker, J. M., & McDonnell, J. J. (2016). Substantial proportion of global streamflow less than three months old. *Nature Geoscience*, *9*(2), 126–129. https://doi.org/10.1038/ngeo2636

Kappelle, M. (2016). Costa Rican ecosystems: A brief summary. *Costa Rican ecosystems*, (October), 709–722.University Press Scholarship Online. https://doi.org/10.7208/chicago/9780226121642.001.0001

Kirchner, J. W. (2003). A double paradox in catchment hydrology and geochemistry. *Hydrological Processes*, *17*(4), 871–874. https://doi.org/10.1002/hyp.5108

Kirchner, J. W. (2016b). Aggregation in environmental systems – Part 2: Catchment mean transit times and young water fractions under hydrologic nonstationarity. *Hydrology and Earth System Sciences*, *20*(1), 299–328. https://doi.org/10.5194/hess-20-299-2016

Kirchner, J. W. (2016a). Aggregation in environmental systems – Part 1: Seasonal tracer cycles quantify young water fractions, but not mean transit times, in spatially heterogeneous catchments. *Hydrology and Earth System Sciences*, *20*(1), 279–297. https://doi.org/10.5194/hess-20-279-2016

Kirchner, J. W. (2019). Quantifying new water fractions and transit time distributions using ensemble hydrograph separation: Theory and benchmark tests. *Hydrology and Earth System Sciences*, *23*(1), 303–349. https://doi.org/10.5194/hess-23-303-2019

Kirchner, J. W., & Knapp, J. L. A. (2020). Technical note: Calculation scripts for ensemble hydrograph separation. *Hydrology and Earth System Sciences*, *24*(11), 5539–5558. https://doi.org/10.5194/hess-24-5539-2020

Klaus, J., & McDonnell, J. J. (2013). Hydrograph separation using stable isotopes: Review and evaluation. *Journal of Hydrology*, *505*, 47–64. https://doi.org/10.1016/j.jhydrol.2013.09.006

Kling, H., Fuchs, M., & Paulin, M. (2012). Runoff conditions in the upper Danube basin under an ensemble of climate change scenarios. *Journal of Hydrology*, *424–425*, 264–277. https://doi.org/10.1016/j.jhydrol.2012.01.011

Knapp, J. L. A., Von Freyberg, J., Studer, B., Kiewiet, L., & Kirchner, J. W. (2020). Concentration-discharge relationships vary among hydrological events, reflecting differences in event characteristics. *Hydrology and Earth System Sciences*, *24*(5), 2561–2576. https://doi.org/10.5194/hess-24-2561-2020

Knighton, J., Saia, S. M., Morris, C. K., Archiblad, J. A., & Walter, M. T. (2017). Ecohydrologic considerations for modeling of stable water isotopes in a small intermittent watershed. *Hydrological Processes*, *31*(13), 2438–2452. https://doi.org/10.1002/hyp.11194

Knutson, T. R., Delworth, T. L., Dixon, K. W., Held, I. M., Lu, J., Ramaswamy, V., … Stouffer, R. J. (2006). Assessment of twentieth-century regional surface temperature trends using the GFDL CM2 coupled models. *Journal of Climate*, *19*(9), 1624–1651. https://doi.org/10.1175/JCLI3709.1

Kuppel, S., Tetzlaff, D., Maneta, M. P., & Soulsby, C. (2018). What can we learn from multi-data calibration of a process-based ecohydrological model? *Environmental Modelling & Software*, *101*, 301–316. https://doi.org/10.1016/j.envsoft.2018.01.001

Kuzdas, C., Warner, B., Wiek, A., Yglesias, M., Vignola, R., & Ramírez-Cover, A. (2016). Identifying the potential of governance regimes to aggravate or mitigate local water conflicts in regions threatened by climate change. *Local Environment*, *21*(11), 1387–1408. https://doi.org/10.1080/13549839.2015.1129604

Kuzdas, C., Wiek, A., Warner, B., Vignola, R., & Morataya, R. (2014). Sustainability appraisal of water governance regimes: The case of Guanacaste, Costa Rica. *Environmental Management*, *54*(2), 205–222. https://doi.org/10.1007/s00267-014-0292-0

Landwehr, J. M., & Coplen, T. B. (2018). Line-conditioned excess: A new method for characterizing stable hydrogen and oxygen isotope ratios in hydrologic systems. *Environmental Earth Sciences*, *77*(6), 132–135. https://doi.org/10.1007/s12665-018-7427-1

Lawrence, S. (1992). The protective role of mountain forests. *GeoJournal*, *27*(1), 13–22.

Macías, J. A., Vargas, E. A., & Sracek, O. (2017). A comparative analysis of two methodologies to estimate well protection zones for transport of viruses from septic tanks in volcanic aquifers in Costa Rica. *Environmental Earth Sciences*, *76*, 1–15. https://doi.org/10.1007/s12665-017-6563-3

Magaña, V., Amador, J. A., & Medina, S. (1999). The midsummer drought over Mexico and Central America. *Journal of Climate*, *12*(6), 1577–1588. https://doi.org/10.1175/1520-0442(1999)012<1577:TMDOMA>2.0.CO;2

Maldonado, T., Alfaro, E., Fallas-López, B., & Alvarado, L. (2013). Seasonal prediction of extreme precipitation events and frequency of rainy days over Costa Rica, Central America, using canonical correlation analysis. *Advances in Geosciences*, *33*, 41–52. https://doi.org/10.5194/adgeo-33-41-2013

Moore, R. D. D. (2005). Slug injection using salt in solution. *Streamline, Watershed Management Bulletin*, *8*(2), 1–6.

Muñoz-Villers, L. E., & McDonnell, J. J. (2012). Runoff generation in a steep, tropical montane cloud forest catchment on permeable volcanic substrate. *Water Resources Research*, *48*(9), 1–17. https://doi.org/10.1029/2011WR011316

Murillo, R. S., Esquivel, L. G. R., Antillón, J. J., & Navarro, J. S. (2019). DOC transport and export in a dynamic tropical catchment. *Journal of Geophysical Research: Biogeosciences*, *124*, 1–15. https://doi.org/10.1029/2018JG004897

McGuire K. J., McDonnell J. J. (2006). A review and evaluation of catchment transit time modeling. *Journal of Hydrology*, *330*(3-4), 543–563. https://doi.org/10.1016/j.jhydrol.2006.04.020

Nash, J. E., & Sutcliffe, J. V. (1970). River flow forecasting through conceptual models part I—A Discussion of principles. *Journal of Hydrology*, *10*, 282–290. https://doi.org/10.1016/0022-1694(70)90255-6

Ortiz-Malavasi, E. (2014). *Atlas de Costa Rica 2014*. Instituto Tecnológico de Costa Rica. Escuela de Ingeniería Forestal. Available from: http://hdl.handle.net/2238/6749.

Osburn, C. L., Oviedo-Vargas, D., Barnett, E., Dierick, D., Oberbauer, S. F., & Genereux, D. P. (2018). Regional groundwater and storms are hydrologic controls on the quality and export of dissolved organic matter in two tropical rainforest streams, Costa Rica. *JGR Biosciences*, *123*, 850–866. https://doi.org/10.1002/2017JG003960

Peña-Arancibia, J. L., Van Dijk, A. I. J. M., Mulligan, M., & Bruijnzeel, L. A. (2010). The role of climatic and terrain attributes in estimating baseflow recession in tropical catchments. *Hydrology and Earth System Sciences*, *14*(11), 2193–2205. https://doi.org/10.5194/hess-14-2193-2010

Piovano, T. I., Tetzlaff, D., Carey, S. K., Shatilla, N. J., Smith, A., & Soulsby, C. (2019). Spatially distributed tracer-aided runoff modelling and dynamics of storage and water ages in a permafrost-influenced catchment. *Hydrology and Earth System Sciences*, *23*(6), 2507–2523. https://doi.org/10.5194/hess-23-2507-2019

Prager S, Rios AR, Schiek B, Almeida JS, & Gonzalez CE. 2020. *Vulnerability to climate change and economic impacts in the agriculture sector in Latin America and the Caribbean—TECHNICAL NOTE No IDB-TN-01985*. Inter-American Development Bank.

Quesada-Chacón, D., Barfus, K., & Bernhofer, C. (2021). Climate change projections and extremes for Costa Rica using tailored predictors from CORDEX model output through statistical downscaling with artificial neural networks. *International Journal of Climatology*, *41*(1), 211–232. https://doi.org/10.1002/joc.6616

Quesada-Román, A., Villalobos-Portilla, E., & Campos-Durán, D. (2021). Hydrometeorological disasters in urban areas of Costa Rica, Central America. *Environmental Hazards*, *20*(3), 264–278. https://doi.org/10.1080/17477891.2020.1791034

Rafiei Emam, A., Kappas, M., Fassnacht, S., & Linh, N. H. K. (2018). Uncertainty analysis of hydrological modeling in a tropical area using

different algorithms. *Frontiers of Earth Science*, *12*(4), 661–671. https://doi.org/10.1007/s11707-018-0695-y

Ramírez-Leiva, A., Sánchez-Murillo, R., Martínez-Cruz, M., Calderón, H., Esquivel-Hernández, G., Delgado, V., … Soulsby, C. (2017). Stable isotopes evidence of recycled subduction fluids in the hydrothermal/volcanic activity across Nicaragua and Costa Rica. *Journal of Volcanology and Geothermal Research*, *345*, 172–183. https://doi.org/10.1016/j.jvolgeores.2017.08.013

Remondi, F., Kirchner, J. W., Burlando, P., & Fatichi, S. (2018). Water flux tracking with a distributed hydrological model to quantify controls on the spatiotemporal variability of transit time distributions. *Water Resources Research*, *54*(4), 3081–3099. https://doi.org/10.1002/2017WR021689

Salas-Navarro, J., Sánchez-Murillo, R., Esquivel-Hernández, G., & Corrales-Salazar, J. L. (2019). Hydrogeological responses in tropical mountainous springs. *Isotopes in Environmental and Health Studies*, *55*(1), 25–40. https://doi.org/10.1080/10256016.2018.1546701

Sánchez-Murillo, R., & Birkel, C. (2016). Groundwater recharge mechanisms inferred from isoscapes in a complex tropical mountainous region. *Geophysical Research Letters*, *43*(10), 1–10. https://doi.org/10.1002/2016GL068888

Sánchez-Murillo, R., & Durán-Quesada, A. M. (2019). Preface to stable isotopes in hydrological studies in the tropics: Ecohydrological perspectives in a changing climate. *Hydrological Processes*, *33*(16), 2160–2165. https://doi.org/10.1002/hyp.13305

Sánchez-Murillo, R., Durán-Quesada, A. M., Birkel, C., Esquivel-Hernández, G., & Boll, J. (2017). Tropical precipitation anomalies and d-excess evolution during El Niño 2014-16. *Hydrological Processes*, *31*(4), 956–967. https://doi.org/10.1002/hyp.11088

Sánchez-Murillo, R., Durán-Quesada, A. M., Esquivel-Hernández, G., Rojas-Cantillano, D., Birkel, C., Welsh, K., … Cobb, K. M. (2019). Deciphering key processes controlling rainfall isotopic variability during extreme tropical cyclones. *Nature Communications*, *10*(1), 1–10. https://doi.org/10.1038/s41467-019-12062-3

Sánchez-Murillo, R., Esquivel-Hernández, G., Birkel, C., Correa, A., Welsh, K., Durán-Quesada, A. M., … Poca, M. (2020). Tracing water sources and fluxes in a dynamic tropical environment: From observations to modeling. *Frontiers in Earth Science*, *8*, 438. https://doi.org/10.3389/feart.2020.571477

Sánchez-Murillo, R., Esquivel-Hernández, G., Corrales-Salazar, J. L., Castro-Chacón, L., Durán-Quesada, A. M., Guerrero-Hernández, M., … Terzer-Wassmuth, S. (2020). Tracer hydrology of the data-scarce and heterogeneous Central American Isthmus. *Hydrological Processes*, *34*(11), 2660–2675. https://doi.org/10.1002/hyp.13758

Sánchez-Murillo, R., Esquivel-Hernández, G., Welsh, K., Brooks, E. S., Boll, J., Alfaro-Solís, R., & Valdés-González, J. (2013). Spatial and temporal variation of stable isotopes in precipitation across Costa Rica: An analysis of historic GNIP records. *Open Journal of Modern Hydrology*, *03*(04), 226–240. https://doi.org/10.4236/ojmh.2013.34027

Sánchez-Murillo, R., Romero-Esquivel, L. G., Jiménez-Antillón, J., Salas-Navarro, J., Corrales-Salazar, L., Álvarez-Carvajal, J., … Birkel, C. (2019). DOC transport and export in a dynamic tropical catchment. *Journal of Geophysical Research: Biogeosciences*, *124*(6), 1665–1679. https://doi.org/10.1029/2018JG004897

Schultz, N. M., Griffis, T. J., Lee, X., & Baker, J. M. (2011). Identification and correction of spectral contamination in 2H/1H and 18O/16O measured in leaf, stem, and soil water. *Rapid Communications in Mass Spectrometry*, *25*(21), 3360–3368. https://doi.org/10.1002/rcm.5236

Seibert, J., Rodhe, A., & Bishop, K. (2003). Simulating interactions between saturated and unsaturated storage in a conceptual runoff model. *Hydrological Processes*, *17*(2), 379–390. https://doi.org/10.1002/hyp.1130

Sheffield, J., & Wood, E. F. (2008). Projected changes in drought occurrence under future global warming from multi-model, multi-scenario, IPCC AR4 simulations. *Climate Dynamics*, *31*(1), 79–105. https://doi.org/10.1007/s00382-007-0340-z

Sidle, F. M., Shimizu, T., Tsuboyama, Y., Noguchi, S., & Hosoda, I. (2000). Stormflow generation in steep forested headwaters: A linked hydrogeomorphic paradigm. *Hydrological Processes*, *14*(3), 369–385.

Sohel, M. S. I., Grau, A. V., McDonnell, J. J., & Herbohn, J. (2021). Tropical forest water source patterns revealed by stable isotopes: A preliminary analysis of 46 neighboring species. *Forest Ecology and Management*, *494*(May), 119355. https://doi.org/10.1016/j.foreco.2021.119355

Soulsby, C., Birkel, C., Geris, J., Dick, J., Tunaley, C., & Tetzlaff, D. (2015). Stream water age distributions controlled by storage dynamics and nonlinear hydrologic connectivity: Modeling with high-resolution isotope data. *Water Resources Research*, *51*(9), 7759–7776. https://doi.org/10.1002/2015WR017888

Soulsby, C., Braun, H., Sprenger, M., Weiler, M., & Tetzlaff, D. (2017). Influence of forest and shrub canopies on precipitation partitioning and isotopic signatures. *Hydrological Processes*, *31*(24), 4282–4296. https://doi.org/10.1002/hyp.11351

Sprenger, M., Stumpp, C., Weiler, M., Aeschbach, W., Allen, S. T., Benettin, P., … Werner, C. (2019). The demographics of water: A review of water ages in the critical zone. *Reviews of Geophysics*, *57*(3), 800–834. https://doi.org/10.1029/2018RG000633

Stewart, M. K., Morgenstern, U., & McDonnell, J. J. (2010). Truncation of stream residence time: How the use of stable isotopes has skewed our concept of streamwater age and origin. *Hydrological Processes*, *24*(12), 1646–1659. https://doi.org/10.1002/hyp.7576

Tognetti, S. S., Aylward, B., & Bruijnzeel, L. A. (2011). Assessment needs to support the development of arrangements for payments for ecosystem services from tropical montane cloud forests. In *Tropical montane cloud forests: Science for conservation and management* (pp. 671–685). Cambridge, U.K: Cambridge University Press. https://doi.org/10.1017/CBO9780511778384.072

Uhlenbrook, S., Frey, M., Leibundgut, C., & Maloszewski, P. (2002). Hydrograph separations in a mesoscale mountainous basin at event and seasonal timescales. *Water Resources Research*, *38*(6), 31-1–31-14. https://doi.org/10.1029/2001WR000938

Uhlenbrook, S., & Hoeg, S. (2003). Quantifying uncertainties in tracer-based hydrograph separations: A case study for two-, three- and five-component hydrograph separations in a mountainous catchment. *Hydrological Processes*, *17*(2), 431–453. https://doi.org/10.1002/hyp.1134

von Freyberg, J., Studer, B., & Kirchner, J. W. (2017). A lab in the field: High-frequency analysis of water quality and stable isotopes in stream water and precipitation. *Hydrology and Earth System Sciences*, *21*(3), 1721–1739. https://doi.org/10.5194/hess-21-1721-2017

Wallbott, L., Siciliano, G., & Lederer, M. (2019). Beyond PES and REDD+: Costa Rica on the way to climate-smart landscape management? *Ecology and Society*, *24*(1), 1–6. https://doi.org/10.5751/ES-10476-240124

West, A. G., Goldsmith, G. R., Matimati, I., & Dawson, T. E. (2011). Spectral analysis software improves confidence in plant and soil water stable isotope analyses performed by isotope ratio infrared spectroscopy (IRIS). *Rapid Communications in Mass Spectrometry: RCM*, *25*(16), 2268–2274. https://doi.org/10.1002/rcm.5126

Westerberg, I. K., & Birkel, C. (2015). Observational uncertainties in hypothesis testing: Investigating the hydrological functioning of a tropical catchment. *Hydrological Processes*, *29*(23), 4863–4879. https://doi.org/10.1002/hyp.10533

Westerberg, I. K., Gong, L., Beven, K. J., Seibert, J., Semedo, A., Xu, C. Y., & Halldin, S. (2014). Regional water balance modelling using flow-duration curves with observational uncertainties. *Hydrology and Earth System Sciences*, *18*(8), 2993–3013. https://doi.org/10.5194/hess-18-2993-2014

Wiegand, B. A., & Schwendenmann, L. (2013). Determination of Sr and Ca sources in small tropical catchments (La Selva, Costa Rica) – A

comparison of Sr and Ca isotopes. *Journal of Hydrology*, *488*, 110–117. https://doi.org/10.1016/j.jhydrol.2013.02.044

Wohl, E., Barros, A., Brunsell, N., Chappell, N. A., Coe, M., Giambelluca, T., … Ogden, F. (2012). The hydrology of the humid tropics. *Nature Climate Change*, *2*(9), 655–662. https://doi.org/10.1038/nclimate1556

Zadroga, F. (1981). The hydrological importance of a montane cloud forest area of Costa Rica. In R. Lal & E. W. Russell (Eds.), *Tropical agricultural hydrology* (pp. 59–73). John Wiley.

Zambrano-Bigiarini, M. (2020). Goodness-of-fit functions for comparison of simulated and observed observed hydrological time series; Package hydroGOF (pp. 1–76). https://github.com/hzambran/hydroGOF

Zanon, C., Genereux, D. P., & Oberbauer, S. F. (2014). Use of a watershed hydrologic model to estimate interbasin groundwater flow in a Costa Rican rainforest. *Hydrological Processes*, *28*(10), 3670–3680. https://doi.org/10.1002/hyp.9917

Zimmermann, A., Francke, T., & Elsenbeer, H. (2012). Forests and erosion: Insights from a study of suspended-sediment dynamics in an overland flow-prone rainforest catchment. *Journal of Hydrology*, *428–429*, 170–181. https://doi.org/10.1016/j.jhydrol.2012.01.039

SUPPORTING INFORMATION

Additional supporting information may be found in the online version of the article at the publisher's website.

How to cite this article: Mayer-Anhalt, L., Birkel, C., Sánchez-Murillo, R., & Schulz, S. (2022). Tracer-aided modelling reveals quick runoff generation and young streamflow ages in a tropical rainforest catchment. *Hydrological Processes*, *36*(2), e14508. https://doi.org/10.1002/hyp.14508